



Characterization of aminobenzylphenols as protein disulfide isomerase inhibitors in glioblastoma cell lines

Andrea Shergalis, Ding Xue, Fatma Z Gharbia, Hannah Driks, Binita Shrestha, Amina Tanweer, Kirin Cromer, Mats Ljungman, and Nouri Neamati

J. Med. Chem., **Just Accepted Manuscript** • DOI: 10.1021/acs.jmedchem.0c00728 • Publication Date (Web): 24 Aug 2020

Downloaded from pubs.acs.org on August 26, 2020

Just Accepted

“Just Accepted” manuscripts have been peer-reviewed and accepted for publication. They are posted online prior to technical editing, formatting for publication and author proofing. The American Chemical Society provides “Just Accepted” as a service to the research community to expedite the dissemination of scientific material as soon as possible after acceptance. “Just Accepted” manuscripts appear in full in PDF format accompanied by an HTML abstract. “Just Accepted” manuscripts have been fully peer reviewed, but should not be considered the official version of record. They are citable by the Digital Object Identifier (DOI®). “Just Accepted” is an optional service offered to authors. Therefore, the “Just Accepted” Web site may not include all articles that will be published in the journal. After a manuscript is technically edited and formatted, it will be removed from the “Just Accepted” Web site and published as an ASAP article. Note that technical editing may introduce minor changes to the manuscript text and/or graphics which could affect content, and all legal disclaimers and ethical guidelines that apply to the journal pertain. ACS cannot be held responsible for errors or consequences arising from the use of information contained in these “Just Accepted” manuscripts.

1
2
3 **Characterization of aminobenzylphenols as protein disulfide**
4
5
6 **isomerase inhibitors in glioblastoma cell lines**
7
8

9
10 *Andrea Shergalis^{†, #}, Ding Xue^{†, #}, Fatma Z. Gharbia[†], Hannah Driks[†], Binita Shrestha[†],*

11
12
13
14 *Amina Tanweer[†], Kirin Cromer[†], Mats Ljungman[‡], Nouri Neamat[†] **
15
16

17
18 [†]Department of Medicinal Chemistry, College of Pharmacy, Rogel Cancer Center, University of
19 Michigan, Ann Arbor, Michigan 48109, United States
20
21

22
23
24 [‡]Department of Radiation Oncology, University of Michigan Medical School and Rogel Cancer
25 Center, School of Public Health, Ann Arbor, Michigan 48109, United States
26
27

28
29
30 **KEYWORDS.** Brain cancer, unfolded protein response, endoplasmic reticulum stress,
31
32
33 cysteine, glutathione, protein disulfide isomerase
34
35
36
37
38
39
40
41
42
43
44
45
46
47
48
49
50
51
52
53
54
55
56
57
58
59
60

ABSTRACT

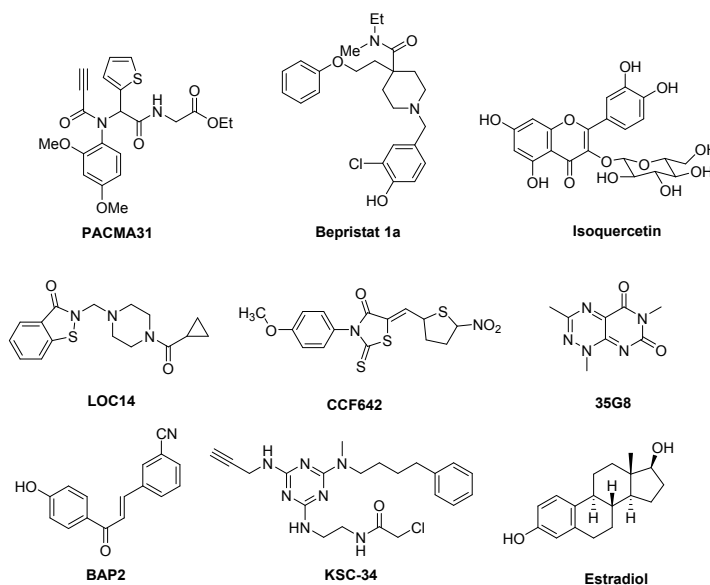
Disulfide bond formation is a critical post-translational modification of newly synthesized polypeptides in the oxidizing environment of the endoplasmic reticulum and is mediated by protein disulfide isomerase (PDIA1). In this study, we report a series of α -aminobenzylphenol analogues as potent PDI inhibitors. The lead compound, **AS15**, is a covalent nanomolar inhibitor of PDI and the combination of **AS15** analogues with glutathione synthesis inhibitor BSO leads to synergistic cell growth inhibition. Using a nascent RNA sequencing we show that an **AS15** analogue triggers the unfolded protein response in glioblastoma cells. A BODIPY-labeled analogue binds proteins including PDIA1, suggesting the compounds are cell-permeable and reach the intended target. Taken together, these findings demonstrate an extensive biochemical characterization of a novel series of highly potent reactive small molecules that covalently bind to PDI.

INTRODUCTION

Glioblastoma (GBM) is the leading primary brain cancer diagnosed in adults.¹ GBM is an aggressive, high-grade glioma with a low 5.6% five-year survival rate. Current standard-of-care – radiation and temozolomide chemotherapy – prolong survival by a few months, but even after remission, the cancer recurs. Thus, innovative therapies are needed to effectively treat GBM.² GBM cells survive by upregulating the protein folding oxidoreductase protein disulfide isomerase (PDIA1, also known as PDI). PDI reduces, oxidizes, and isomerizes disulfide bonds in nascent polypeptides and other substrates *via* two catalytic CGHC active sites that sit 15–30 Å apart in two homogenous domains.³ PDI is overexpressed in several cancers to meet the increased demands in protein synthesis.⁴⁻⁶

The **a** and **a'** domains of PDI are connected by **b** and **b'** domains, which share identity with the **a** and **a'** domains, but do not contain the CGHC active sites. As evidenced by the pK_a values, the N-terminal cysteine in each **a** and **a'** domain active site (Cys53 and Cys397) is stabilized in the thiolate form, while the C-terminal cysteine thiolate is destabilized. This allows the nucleophilic N-terminal cysteines to attack substrates and form mixed disulfides. The C-terminal cysteines more selectively react with the N-terminal cysteines, mediated in the **a** domain by the pK_a of Cys56 that is lowered by the local environment, containing a conserved Arg120.⁷ This reaction generates a reduced substrate and disulfide in PDI.

The thiolate form of the redox active N-terminal cysteines reacts with electrophilic compounds. Thus, many electrophilic compounds have been identified as covalent PDI inhibitors, including **PACMA31**⁸, **KSC-34**⁹, 3,4-methylenedioxy- β -nitrostyrene (MNS)¹⁰, and **16F16**¹¹ (**Figure 1**). **PACMA31**, an irreversible inhibitor of PDI, demonstrated *in vivo* efficacy in a mouse model of ovarian cancer.¹² Furthermore, **PACMA31** synergized with the multi-kinase inhibitor sorafenib in a mouse model of hepatocellular carcinoma.¹³ One of the main challenges of characterizing the many PDI inhibitors identified to date, recently emphasized by Foster, et al., is competition with endogenous levels of glutathione.¹⁴ Active site PDI inhibitors, especially reactive electrophiles such as **PACMA31**, may compete with glutathione for binding the cysteine thiols of PDI. This strategy is further confounded by the fact that several PDI family members share similar active site motifs, and although the CGHC active site is one of the most reactive of the thioredoxin superfamily, electrophiles that bind this site may also bind to other CxxC-containing PDI family members. One strategy to mitigate off-target toxicity of cysteine-reactive active site inhibitors is to develop more selective inhibitors.¹⁵



1
2
3 **Figure 1.** Previously reported PDI inhibitors studied in the context of ovarian cancer (**PACMA31**),
4
5
6 Huntington's disease (**LOC14**), brain cancer (**BAP2** and **35G8**), thrombosis (**Bepristat 1a** and
7
8 **isoquercetin**), and multiple myeloma (**CCF642**). **KSC-34** is an α -site selective probe and estradiol is an
9
10 endogenous ligand of PDIA1.
11
12
13
14
15
16
17
18

19
20 In addition to the increased PDI expression, GBM cells upregulate the antioxidant
21
22 defense system and are increasingly dependent on glutathione as the tumor grows.¹⁶
23
24
25

26 Glutathione is one of the most abundant molecules in the cell, with concentrations of reduced
27
28 glutathione (GSH) estimated to reach up to 10 mM in cellular compartments. The tripeptide
29
30 composed of glutamic acid, glycine, and cysteine is a key redox buffer and antioxidant molecule
31
32 involved in many cellular processes including reactive oxygen species removal, signal
33
34 transduction, and protein synthesis.¹⁷ Although the total glutathione concentration is similar in the
35
36 cytosol and ER, the ratio of reduced to oxidized glutathione dictates its role in each compartment.
37
38 In the cytosol, glutathione is present mainly in its reduced form, with a ratio of GSH:GSSG of
39
40 ~50,000:1; the ER is a more oxidizing compartment, with an estimated GSH:GSSG ratio of less
41
42 than 7:1.¹⁸ Because of this environment, PDIA1 is present in its disulfide form, poised to accept
43
44 electrons from the reduced thiols in nascent polypeptides. The oxidizing environment of the ER
45
46 aids in protein folding and disulfide bond formation.
47
48
49
50
51

52 The initial goal of this study was to characterize a new class of PDI inhibitors in the context
53
54 of GBM. Via a medium-throughput biochemical screen, we identified a series of α -
55
56
57
58
59
60

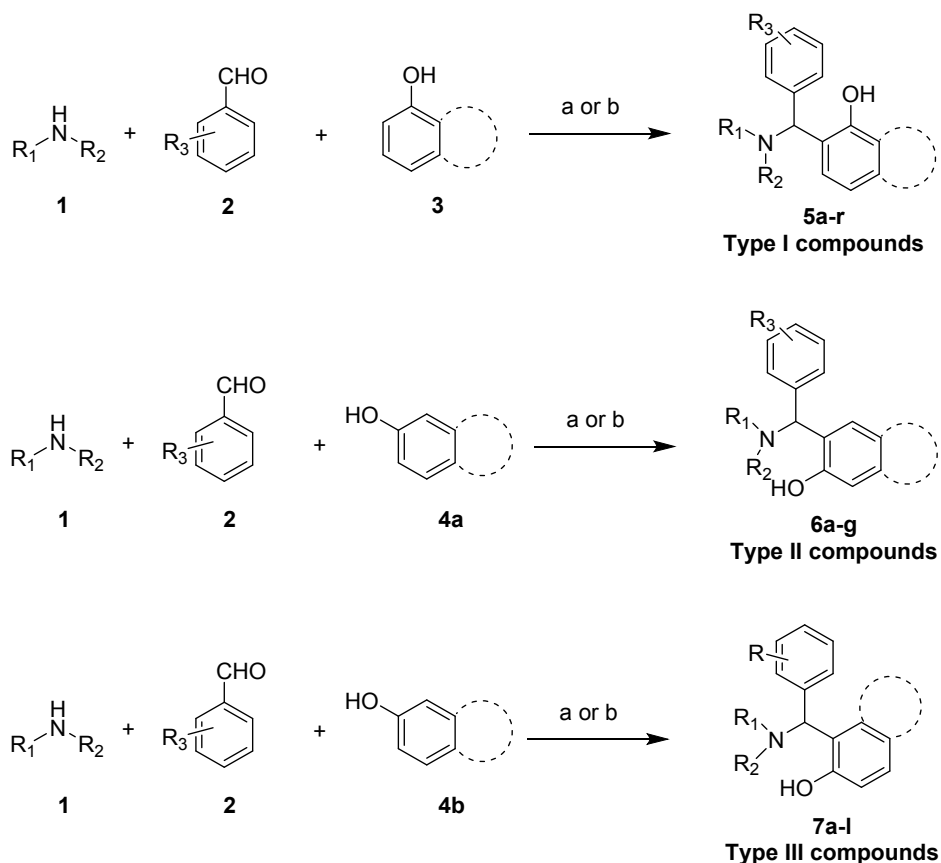
1
2
3 aminobenzylphenols as inhibitors of PDI that possibly target the active site cysteines of PDI via a
4 retro-Michael addition reaction. Similar compounds have been reported for multiple targets,
5
6 including HDACs¹⁹, MIF tautomerase²⁰⁻²³, STAT3/5²⁴, and frataxin²⁵, among others. This finding
7
8 suggested that these inhibitors may not be selective for a single protein in the cells. However, we
9
10 synthesized a BODIPY-labeled analogue that did not bind any of the previously published targets.
11
12 Binding was enhanced when the cells were pre-treated with BSO, suggesting that the efficacy
13
14 may be lowered by intracellular glutathione. Additionally, potency in cells increased with BSO
15
16 treatment. Thus, the compounds are cell-permeable, and cytotoxicity is enhanced with glutathione
17
18 depletion. In all, this study represents the importance of validating in-cell target engagement early
19
20 in the drug discovery process and provides extensive characterization of a class of thiol-reactive
21
22 small molecules.
23
24
25
26
27
28
29

30 RESULTS

31
32
33
34 **Chemistry.** Most of the compounds in the present study were synthesized via a well-established
35
36 Betti reaction employing a phenolic compound, an aldehyde, and an amine in a one-pot fashion.²⁶
37
38 ²⁷ Reactions were either heated in toluene at 100 °C or in EtOH under microwave irradiation at
39
40 120 °C for 30 min depending on the electronic nature of the phenolic starting material. Typically,
41
42 simple phenols, hydroxy naphthalenes, and hydroxy quinolones can be used in such reactions,
43
44 whereas the reactivity of other hydroxy heterocyclic structures remains uncertain. In our study,
45
46 depending on the substitution pattern and electronic properties of the starting materials, three
47
48 different types of products were generated (**Scheme 1**). For starting materials represented by **3**,
49
50 Type I compounds were obtained unambiguously, while with **4a/4b**, electrophilic replacement
51
52 could occur at two distinct *ortho* positions of the hydroxy, leading to either Type II or Type III
53
54
55
56
57
58
59
60

1
2
3 compounds. We found that regioselectivity was strongly related to the electronic properties of the
4
5 bicyclic heterocycles: electron-efficient compounds tend to generate Type II compounds, and
6
7 electron-deficient compounds generate Type III compounds.
8
9

10
11 **Scheme 1.** Synthesis of the compounds with modified Betti reaction.^a
12

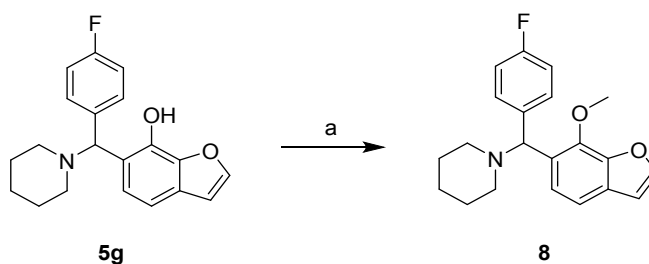


41
42 ^aReagents and conditions: a) Toluene, 100 °C; b) EtOH, 120 °C microwave or conventional
43 heating.
44
45
46
47
48
49

50 Compound **8** was prepared by direct methylation of **5g** with dimethyl sulfate (**Scheme 2**).
51
52 Compound **13**, with a cyclohexane in place of the piperidine moiety, was synthesized by a
53
54 four-step strategy (**Scheme 3**). Benzo[*d*][1,3]dioxol-5-ol (**9**) was reacted with benzoyl chloride by
55
56
57
58
59
60

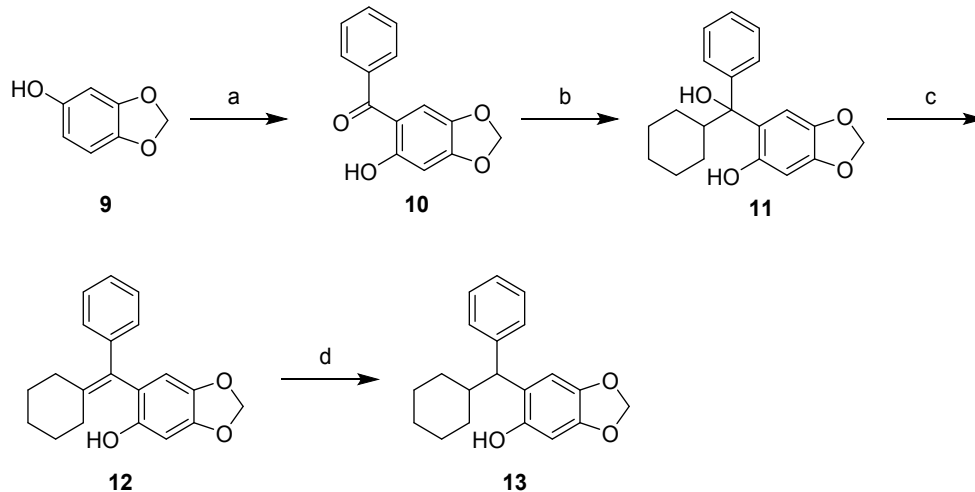
1
2
3 an *ortho*-selective electrophilic attack facilitated by a highly coordinating metal phenolate
4 intermediate generated *in situ*.^{28, 29} The diaryl ketone **10** was reacted with cyclohexylmagnesium
5 bromide to give tertiary alcohol **11**. A TsOH-catalyzed elimination afforded **12**, and **12** was
6 subjected to catalytic hydrogenation to give **13**.
7
8
9
10
11
12

13 **Scheme 2.** Synthesis of compound **8**.^a
14



28 ^aReagents and conditions: a) Me₂SO₄, K₂CO₃, acetone.
29

30 **Scheme 3.** Synthesis of compound **13**.^a
31



^aReagents and conditions: a) i, MeI, Mg, Et₂O, ii, benzoyl chloride; b) cyclohexylmagnesium bromide, THF, rt–50 °C; c) p-TsOH, toluene, rt; d) Pd/C, H₂, EtOH, 60 °C.

1
2
3 **Lead Compound AS15 Is a Nanomolar Inhibitor of PDI.** A screening campaign of 1000 highly
4 diverse compounds from the National Cancer Institute at 40 μM in the PDI reductase assay
5 afforded almost 200 compounds that inhibited 50% of PDI activity (**Figure 2A**). Those compounds
6 were screened for cytotoxicity in U-87 MG and MIA PaCa-2 cell lines, and compounds with >
7 40% inhibition of cell growth at 30 μM were subjected to dose response assays in both the 3-(4,5-
8 dimethylthiazol-2-yl)-2,5-diphenyltetrazolium bromide (MTT) and PDI reductase assays. **AS15**
9 and **CD343** emerged as lead scaffolds with IC_{50} values in the PDI reductase assay of 300 ± 90 nM
10 and 170 ± 50 nM, respectively (**Figure 2B-C**). When a residue in the **b'** domain of PDI important
11 for substrate binding, Histidine 256, was mutated to an alanine residue, both **AS15** and **CD343**
12 retained their activity (**Figure S1A**). This result suggested **AS15** and **CD343** activity was not
13 dependent on the substrate-binding domain. Thus, we focused on determining whether inhibition
14 was based on the interaction between **AS15** and **CD343** and the active-site cysteines. **AS15** and
15 **CD343** inhibited activity of PDIA2 and, to a lesser extent, PDIA3 (**Figure S1B**). The lead
16 compounds decreased viability of U-87 MG cells with IC_{50} values of 18.3 ± 9.2 μM for **AS15** and
17 10.6 ± 0.7 μM for **CD343** (**Figure S1C**). Interaction with oxidized PDI was further probed with
18 the thermal shift assay; however, **AS15** and **CD343** did not stabilize PDI to thermal degradation,
19 similar to **PACMA31** (**Figure 2D**). These initial results suggested that the compounds inhibit PDI
20 as thiol-reactive compounds and not via the substrate-binding domain like estradiol or **BAP2**.³⁰
21
22
23
24
25
26
27
28
29
30
31
32
33
34
35
36
37
38
39
40
41
42
43
44
45
46
47
48
49
50
51
52
53
54
55
56
57
58
59
60

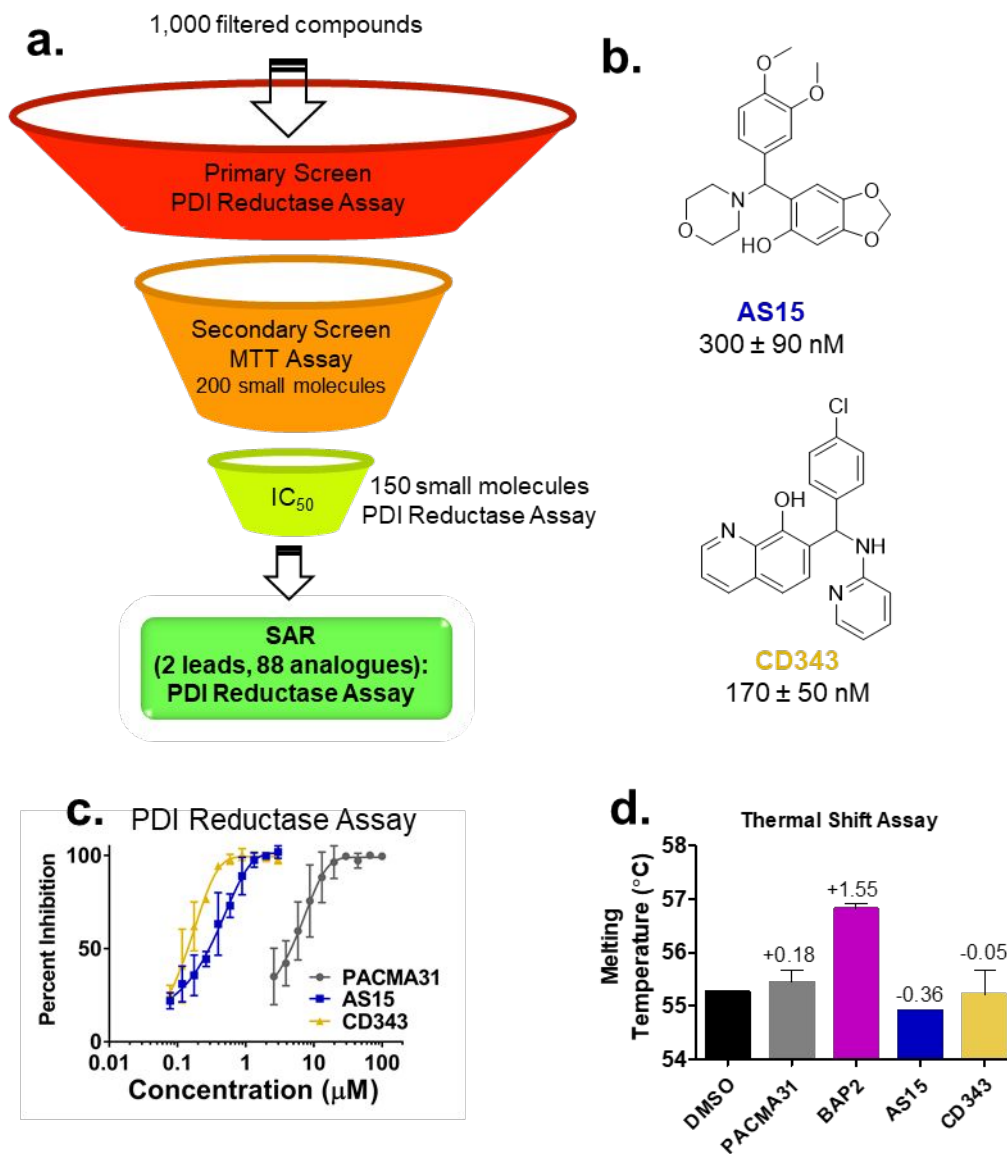


Figure 2. (a) Screening approach leading to the discovery of **AS15** and **CD343**. (b) Structures of **AS15** and **CD343**, and IC₅₀ values calculated in the PDI reductase assay. (c) Dose–response curves of **PACMA31**, **AS15**, and **CD343** in the PDI reductase assay. (d) Shifts in the melting temperatures of **PACMA31**, **AS15**, and **CD343** in the thermal shift assay. SAR: structure–activity relationship.

Structure–Activity Relationships Reveal AS15 Analogues Are Not Substrate–Binding

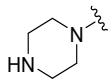
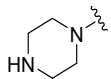
Domain Inhibitors. To further assess the mechanism of inhibition of AS15 and CD343 and determine the structural requirements for their activity, we obtained 89 analogues from Chem Div libraries and the NCI Developmental Therapeutics Program and tested their potency in the PDI reductase assay (**Tables 1–4**). Compounds were tested for purity, and only compounds with purity > 95% were used for structure–activity relationship analysis. Generally, all AS15 and CD343 analogues possess an α -aminobenzylphenol core that consists of phenolic, amino, and phenyl moieties. While the phenolic moiety is limited to 5-hydroxybenzo[*d*][1,3]dioxole (AS15 analogues) or 8-hydroxyquinoline (CD343 analogues), the amino and phenyl moieties are diversified. For compounds with the 5-hydroxybenzo[*d*][1,3]dioxole moiety, a variety of cyclic amines including morpholine, piperidine, piperazine, and pyrrolidine were incorporated. Most of the compounds inhibited PDI with IC₅₀ values below 1 μ M, and different halogens and electron–donating groups such as chloro, fluoro, methoxy, amino, and hydroxy on the phenyl ring were well–tolerated. Some of the compounds showed moderate cytotoxicity with IC₅₀ values of 10–30 μ M; however, correlation with PDI inhibition was not observed (**Table 1**). Aromatic amines such as aminopyridine, aminopyrimidine, and imidazole were generally tolerated, and PDI inhibition was comparable to those with saturated cyclic amines. Ureas were not tolerated and led to a complete loss of activity, possibly because of their loss of basicity that contributed to PDI binding (**Table 2**). Compounds without the bicyclic aromatic core or hydroxy group were inactive against PDI and non–toxic (**Figure S2**). Furthermore, compounds without the tertiary amine were inactive against PDI and were non–toxic, with the exception of tri–methoxy substituents on the aromatic ring (**Table S1**). CD analogues possess the 8-hydroxyquinoline core along with an aromatic amine such as 2-aminopyridine or aniline, and their ability to inhibit PDI activity was

comparable to the **AS15** analogues, except that the 4-methyl substitution of the pyridine was not compatible when methyl or chloro was present on the phenyl moiety. Interestingly, many of these compounds showed stronger cytotoxicity with IC₅₀ values as low as 2.1 ± 0.1 μM (**Tables 3 and 4**).

Table 1. SAR of Compounds with 5-Hydroxybenzo[*d*][1,3]dioxole and Saturated Cyclic Amine Moieties

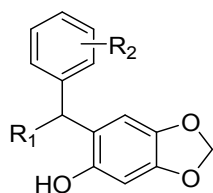


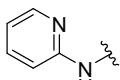
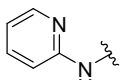
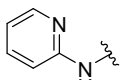
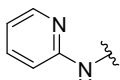
compound	NSC Number	R ₁	R ₂	PDI IC ₅₀ (μM) ^a	MTT IC ₅₀ (μM) ^b
AS15/NC014	368252		3,4-di-OCH ₃	0.30 ± 0.09	18.3 ± 9.2
NC016	368260		3,4,5-tri-OCH ₃	0.64 ± 0.31	> 10
NC133	381577		2,4,6-tri-OCH ₃	0.98 ± 0.30	13.6 ± 1.7
NC107	368248		3,4-OCH ₂ O-	< 0.2	> 30
NC108	368256		2-OH, 3-OCH ₃	0.90 ± 0.75	> 10
NC110	368261		3-OCH ₃ , 4-OH	0.23 ± 0.11	27.1 ± 2.4
NC161	364724		4-OCH ₃	0.13 ± 0.06	> 10
NC134	381579		2-OCH ₃	0.33 ± 0.05	27.7 ± 2.7
NC115	368275		4-Cl	0.092 ± 0.023	> 30
NC117	368277		4-F	0.23 ± 0.06	> 30
NC141	667921		2-OH	0.34 ± 0.09	> 30
NC018	368267		3,4-di-OCH ₃	0.96 ± 1.08	24.8 ± 1.2
NC015	368253		3, 4, 5-tri-OCH ₃	0.70 ± 0.13	> 10
NC022	368274		4-OCH ₃	0.88 ± 0.36	28.3 ± 1.6
NC020	368273		4-N(CH ₃) ₂	1.27 ± 0.34	24.7 ± 2.4

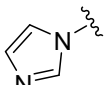
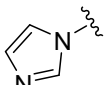
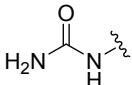
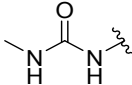
NC024	370278		2,4-di-OCH ₃	2.59 ± 1.84	> 30
NC162	368254		3,4-OCH ₂ O-	0.35 ± 0.11	> 10
NC116	368276		4-F	0.27 ± 0.04	> 30
NC120	369090		4-OH	0.68 ± 0.35	> 30
NC025	370279		2,4-di-OCH ₃	0.36 ± 0.05	> 30
NC026	370281		4-OCH ₃	1.52 ± 0.02	22.6 ± 5.9
NC027	370283		4-N(CH ₃) ₂	< 0.20	> 30
NC028	370285		2-OH, 3-OCH ₃	1.65 ± 0.65	> 10
NC122	370280		4-F	< 0.20	> 30
NC123	370282		3,4-OCH ₂ O-	0.023 ± 0.017	> 30
NC124	370284		3,4,5-tri-OCH ₃	0.18 ± 0.02	24.2 ± 7.1

^aInhibition of PDI was assessed by PDI reductase assay. IC₅₀ values are indicated as the mean ± SD (standard deviation) of at least three independent experiments. ^bMTT cytotoxicity IC₅₀ values were determined in U-87 MG cells.

Table 2. SAR of Compounds with 5-Hydroxy benzo[*d*][1,3]dioxole and Other Amine Moieties

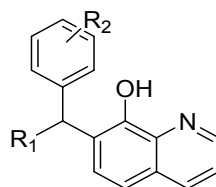


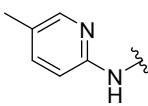
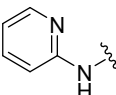
compound	NSC Number	R ₁	R ₂	PDI IC ₅₀ (μM) ^a	MTT IC ₅₀ (μM) ^b
NC163	368255		3,4-OCH ₂ O-	0.072 ± 0.017	> 10
NC300	368281		3,5-di-OCH ₃ , 4-OH	0.17 ± 0.04	> 10
NC017	368265		3,4-OCH ₂ O-	1.18 ± 0.11	> 10
NC019	368270		4-OCH ₃	1.30 ± 0.39	> 10
NC165	368268		2-OH, 3-OCH ₃	9.02 ± 4.61	> 10
NC299	368279		3,5-di-OCH ₃ , 4-OH	2.20 ± 0.53	> 10

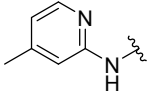
NC166	368278		4-F	12.72 ± 3.47	> 10
NC118	368280		4-F	0.67 ± 0.14	> 10
NC119	369087		4-OCH ₃	0.62 ± 0.04	> 10
NC023	369678		4-OH	> 40	> 10
NC029	371006		3,4-OCH ₂ O-	> 40	> 10
NC030	371007		3,4,5-tri-OCH ₃	> 40	> 10
NC168	371005		4-F	> 30	> 10

^aInhibition of PDI was assessed by PDI reductase assay. IC₅₀ values are indicated as the mean ± SD (standard deviation) of at least three independent experiments. ^bMTT cytotoxicity IC₅₀ values were determined in U-87MG cells.

Table 3. SAR of compounds with 8-Hydroxyquinoline and 2-Aminopyridine Moieties

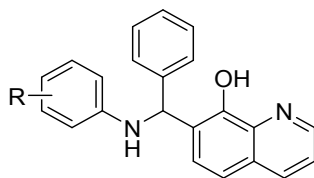


compound	ID	R ₁	R ₂	PDI IC ₅₀ (μM) ^a	MTT IC ₅₀ (μM) ^b
CD528	G856-2528		3,5-di-OCH ₃ , 4-OH	0.18 ± 0.06	7.4 ± 1.2
CD343	4896-2958		4-Cl	0.17 ± 0.05	10.6 ± 0.7
CD345	4896-3004		2,6-di-Cl	1.89 ± 0.31	6.9 ± 1.6
CD639	7706-0076		2-Cl	0.50 ± 0.17	9.4 ± 0.6
CD611	4896-3086		4-CH ₃	0.46 ± 0.07	> 10
CD344	4896-3003		4-CH ₂ CH ₃	0.17 ± 0.12	9.3 ± 5.9
CD346	4896-3082		2,5-di-CH ₃	0.73 ± 0.12	13.8 ± 5.9
CD355	4896-4013		2,4,6-tri-CH ₃	0.19 ± 0.09	10 ± 0.6
CD638	4896-3084		3-OCH ₃	2.86 ± 2.37	11.9 ± 0.4
CD626	G856-2546		2-F	0.47 ± 0.17	> 10

CD613	5994-0466		2-Cl, 3-OH	0.37 ± 0.03	> 10
NC272	1014		–	< 0.20	> 10
CD354	4896-4000		2-CH ₃	> 40	> 10
CD361	5994-0131		2,5-di-CH ₃	> 40	> 10
CD350	4896-3501		4-F	0.14 ± 0.06	> 10
CD377	7706-0074		2-F	0.88 ± 0.23	13.1 ± 3.5
CD341	4896-0018		2-F, 6-Cl	> 40	20.6 ± 7.8
CD373	7033-0321		3-F	0.35 ± 0.07	9.2 ± 0.4
CD348	4896-3250		2-Cl	> 40	9.9 ± 1.4
CD349	4896-3254		2,6-di-Cl	> 40	7.2 ± 2.2
CD352	4896-3773		4-OBn	0.62 ± 0.29	9.3 ± 0.9
CD362	5994-0331		4-CH ₂ CH ₃	5.39 ± 0.68	8.9 ± 2.2
CD601	G856-2531		4-CF ₃	26.50 ± 19.15	2.1 ± 0.1
CD363	5994-0397		4-NO ₂	0.53 ± 0.15	3.4 ± 0.6
CD594	5704-0657		3-OH, 4-OCH ₃	0.15 ± 0.02	> 10

^aInhibition of PDI was assessed by PDI reductase assay. IC₅₀ values are indicated as the mean ± SD (standard deviation) of at least three independent experiments. ^bMTT cytotoxicity IC₅₀ values were determined in U-87MG cells.

Table 4. SAR of Compounds with 8-Hydroxyquinoline and Aniline Moieties



compound	NSC Number	R	PDI IC ₅₀ (μM) ^a	MTT IC ₅₀ (μM) ^b
NC266	1008	–	0.11 ± 0.04	> 10
NC268	1010	4-NO ₂	0.15 ± 0.05	> 10
NC269	1011	4-COOH	0.30 ± 0.05	> 10
NC270	1012	2-COOH	1.48 ± 1.52	> 10
NC273	1015	2-COOC ₂ H ₅	< 0.20	> 10

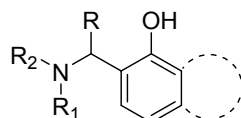
NC282	84087	2-OCH ₃	0.39 ± 0.11	> 10
-------	-------	--------------------	-------------	------

^aInhibition of PDI was assessed by PDI reductase assay. IC₅₀ values are indicated as the mean ± SD (standard deviation) of at least three independent experiments. ^bMTT cytotoxicity IC₅₀ values were determined in U U-87MG cells.

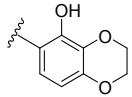
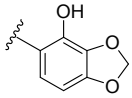
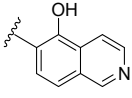
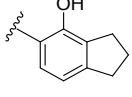
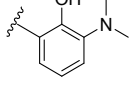
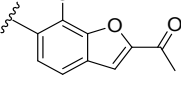
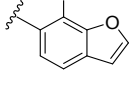
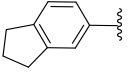
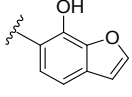
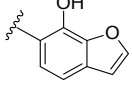
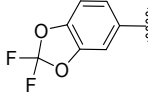
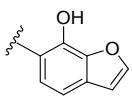
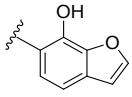
Having explored the SAR around the amino and phenyl moieties, which generally had a nominal impact on PDI inhibition, we synthesized and tested an additional 38 compounds to diversify the phenolic moiety and probe the impact on PDI inhibition. Notably, this is also the first exploration of the reactivity and regioselectivity of a variety of hydroxy bicyclic heterocycles in Betti-style reactions and the biological activity of their products. Compounds were classified into three types based on the substitution pattern on the phenolic moiety. Type I compounds have a similar substitution pattern as **CD343** (**Table 5**). The results indicated that 8-hydroxyquinazoline (**5c-d**), 5-hydroxyquinoxaline (**5e**), 4-hydroxybenzothiazole (**5f**), 7-hydroxybenzofuran (**5g**), 5-hydroxy-1,4-benzodioxane (**5h**), 4-hydroxybenzo[*d*][1,3]dioxole (**5i**), and 5-hydroxyisoquinoline (**5j**) are all well tolerated. **5h** has the highest potency with an IC₅₀ value of 290 ± 120 nM. The incorporation of 4-indanol (**5k**) led to a complete loss of the potency, indicating a H-bond acceptor might be essential. The fact that **5i** lost activity despite containing a H-bond acceptor suggests a bicyclic structure is necessary to fulfill the steric requirement around this moiety. Using **5g** as a model compound, different substituents were introduced. All substituents were well-tolerated, and **5p** and **5q** exhibited IC₅₀ values below 0.2 μM. For Type II compounds with a similar substitution pattern as **AS15** (**Table 6**), both 5-hydroxybenzo[*d*][1,3]dioxole and 6-hydroxy-1,4-benzodioxane are preferred, with 6-hydroxyindoline leading to a moderate loss of activity (**6d**). Similar to **5k** in the **CD series**, compounds **6f** and **6g** completely lost activity. Type III compounds with substitution patterns different from **AS15** and **CD343** were also synthesized by incorporating different phenolic moieties (**Table 7**). The majority of the compounds lost their

activity, suggesting an unfavorable binding mode. The exceptions included compounds containing a 5-hydroxyindole or 5-hydroxyindazole, with the latter leading to comparable inhibition of PDI at sub-micromolar IC_{50} values for all of its analogues. It is possible that in this case the -NH group of indole/indazole forms additional interactions with PDI as a H-bond donor. Most of the synthesized α -aminobenzylphenols were not cytotoxic at 30 μ M, which was similar to the trend observed with the NC and CD series (Tables 5–7).

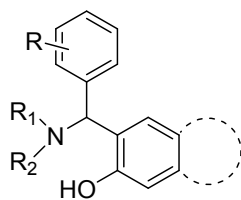
Table 5. SAR of Type I Compounds



compound	R	R ₁ -N-R ₂	phenol moiety	PDI IC ₅₀ (μ M) ^a	MTT (% inhibition at 30 μ M) ^b
5a	2,3-OMe-Ph			0.39 \pm 0.03	74 (IC ₅₀ : 33 μ M)
5b	4-F-Ph			0.69 \pm 0.13	54 (IC ₅₀ : 37 μ M)
5c	4-F-Ph			4.86 \pm 2.04	32
5d	4-F-Ph			1.20 \pm 0.51	44
5e	4-F-Ph			0.66 \pm 0.13	0
5f	4-F-Ph			0.57 \pm 0.25	0
5g	4-F-Ph			0.56 \pm 0.13	0

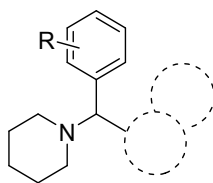
1						
2						
3						
4	5h	4-F-Ph			0.29 ± 0.12	0
5						
6						
7						
8	5i	4-F-Ph			2.83 ± 1.26	0
9						
10						
11						
12	5j	4-F-Ph			0.61 ± 0.20	0
13						
14						
15						
16	5k	4-F-Ph			> 10	28
17						
18						
19	5l	4-F-Ph			> 30	0
20						
21						
22						
23	5m	4-F-Ph			1.23 ± 0.23	0
24						
25						
26						
27	5n	2-OH,4-F-Ph			1.07 ± 0.01	0
28						
29						
30						
31	5o				0.41 ± 0.11	5
32						
33						
34						
35	5p				< 0.2	1
36						
37						
38						
39	5q				< 0.2	9
40						
41						
42	5r	4-CF ₃ -Ph			0.30 ± 0.03	5
43						
44						

^aInhibition of PDI was assessed by PDI reductase assay. IC₅₀ values are indicated as the mean \pm SD (standard deviation) of at least three independent experiments. ^bMTT cytotoxicity determined in U-87 MG cells.

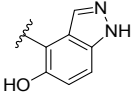
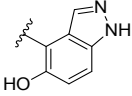
Table 6. SAR of Type II Compounds

compound	R	R ₁ -N-R ₂	phenol moiety	PDI IC ₅₀ (μM) ^a	MTT (% inhibition at 30 μM) ^b
6a	2,3-OMe			1.06 ± 0.31	66 (IC ₅₀ : 32 μM)
6b	H			2.9 ± 2.4	17 ^c
6c	4-F			0.67 ± 0.29	1
6d	4-F			7.01 ± 1.39	0
6e	2,3-OMe			0.51 ± 0.13	40
6f	4-F			> 30	13
6g	4-F			> 100	0

^aInhibition of PDI was assessed by PDI reductase assay. IC₅₀ values are indicated as the mean ± SD (standard deviation) of at least three independent experiments. ^bMTT cytotoxicity determined in U-87 MG cells. ^cMTT cytotoxicity determined in A-172 cells.

Table 7. SAR of Type III Compounds

compound	R	phenol moiety	PDI IC ₅₀ (μM) ^a	MTT (% inhibition at 30 μM) ^b
7a	4-F		> 30	10
7b	4-F		> 100	1
7c	4-F		> 100	0
7d	4-F		10.20 ± 2.88	0
7e	4-F		>100	0
7f	4-F		1.81 ± 0.06	0
7g	4-F		0.35 ± 0.14	87
7h	4-CF ₃		0.71 ± 0.10	0
7i	4-NO ₂		0.52 ± 0.36	0
7j			0.34 ± 0.26	0

7k			0.29 ± 0.13	0
7l			0.83 ± 0.29	0

^aInhibition of PDI was assessed by PDI reductase assay. IC₅₀ values are indicated as the mean \pm SD (standard deviation) of at least three independent experiments. ^bMTT cytotoxicity determined in U-87 MG cells.

AS15 Analogues Covalently Bind to PDI. We addressed the importance of the phenolic hydroxy and amine moieties of the series with two compounds; **8** lost activity with the replacement of the phenolic hydroxy (**5g**) with a methoxy (**Figure 3A**). Similarly, replacing the piperidine in **6b** with a cyclohexane abolished its PDI inhibition (**13**) (**Figure 3B**). Both compounds demonstrated the importance of the α -aminobenzylphenol core to the potency of this series of compounds.

Due to the nature of disulfide bonds, we hypothesized that the **AS15** analogues may be attacked by the nucleophilic cysteine thiols in the active sites of reduced PDI, as is the case for other electrophilic PDI inhibitors. Upon a reaction that exposes the Michael acceptor, the free thiol on PDI could react and form a covalent adduct (**Figure 3C**). This type of retro Michael addition to protein thiols has been observed with hydroxyquinolines like **CD343**.¹⁹ A zinc-dependent mechanism opened a quinone methide for selective reaction with HDAC5 and HDAC9¹⁹, another quinone methide intermediate was found to react with protein thiols over forming DNA adducts³¹, and co-crystallization confirmed pyridinylmethyl quinoline fragment binding to MIF tautomerase *via* a proline residue.²⁰ In the case of the pyridinylmethyl quinoline fragment, the compound bound *via* a retro Michael addition reaction that formed the quinone methide intermediate. This intermediate was primed to undergo the aza-Michael addition to covalently link to a proline residue in MIF tautomerase.

1
2
3 To confirm **AS15** analogues covalently label PDI, we incubated 10 μM PDI with 100 μM
4 DTT and 100 μM **6a** or **6f** and monitored adduct formation with quadrupole time-of-flight mass
5 spectrometry (QTOF). We found that the fragment matching the proposed mechanism of action
6 was apparent rapidly after the compound was added (**Figure 3D**). **6a** bound reduced PDI at three
7 sites. Recombinant PDI contains six cysteines, four of which form disulfide bonds when oxidized.
8 When **6a** was incubated in a mixture of 1:1:1 PDI:GSTO1:GRP78, the mass of PDI increased by
9 two equivalents of the fragment, demonstrating that **6a** can bind PDI in the presence of competing
10 proteins (**Figure 3E**, **Figure S3A**). An inactive analogue of **6a** without the aromatic benzoxole
11 (**6f**) did not demonstrate covalent binding to PDI under the same conditions (**Figure S3B**).
12
13
14
15
16
17
18
19
20
21
22
23

24 To assess the covalent binding nature, we measured the $k_{\text{inact}}/K_{\text{I}}$ of the lead compounds in
25 the PDI reductase assay with reduced PDI. For covalent inhibitors, the $k_{\text{inact}}/K_{\text{I}}$ is the ratio of the
26 observed rate of inactivation after a reversible reaction to form a protein-inhibitor (P-I) complex
27 with all the protein molecules (k_{inact}) to the concentration of inhibitor required to reach half of the
28 maximum rate of covalent bond formation (K_{I}). The kinetics of covalent PDI inhibitors **16F16**,
29 **PACMA31**, and **AS15** were measured by assessing activity in the PDI reductase assay at
30 incubation times from 5 to 60 minutes. **AS15** inhibited PDI with a $k_{\text{inact}}/K_{\text{I}}$ of $2.6 \times 10^3 \text{ M}^{-1}\text{s}^{-1}$
31 (**Figure 3F**). $k_{\text{inact}}/K_{\text{I}}$ for **PACMA31** was $2.0 \times 10^2 \text{ M}^{-1}\text{s}^{-1}$ and $k_{\text{inact}}/K_{\text{I}}$ for **16F16** was 1.7×10^2
32 $\text{M}^{-1}\text{s}^{-1}$. Thus, **AS15** was more efficient at inhibiting PDI than both covalent inhibitors **PACMA31**
33 and **16F16**. Furthermore, a gel-based competition assay with the fluorescent probe of **PACMA31**,
34 **PACMA57**, confirmed **AS15** analogues could compete with **PACMA57** to bind PDI (**Figure**
35 **3G**).¹² Because **PACMA57** binds PDI at either Cys397 or Cys400, this suggests that **AS15** can
36 also bind one of these cysteines. Inactive analogue **6f** did not compete with **PACMA57** for binding
37 to PDI.
38
39
40
41
42
43
44
45
46
47
48
49
50
51
52
53
54
55
56
57
58
59
60

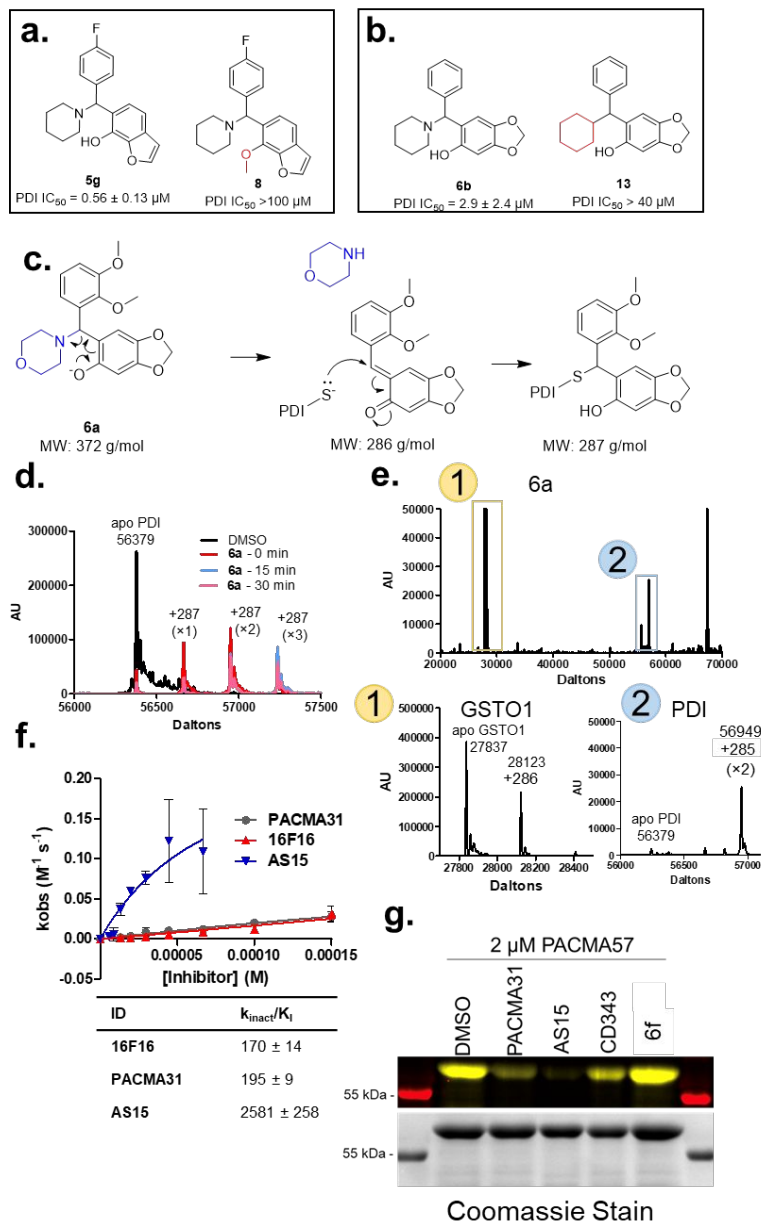


Figure 3. Structure–activity relationship indicates that compounds are covalent PDI inhibitors. (a)

Comparison of compounds with free hydroxy or methoxy on the bicyclic moiety. (b) Comparison of

compounds with piperidine or cyclohexane moiety. (c) Proposed mechanism of inhibition *via* retro–Michael

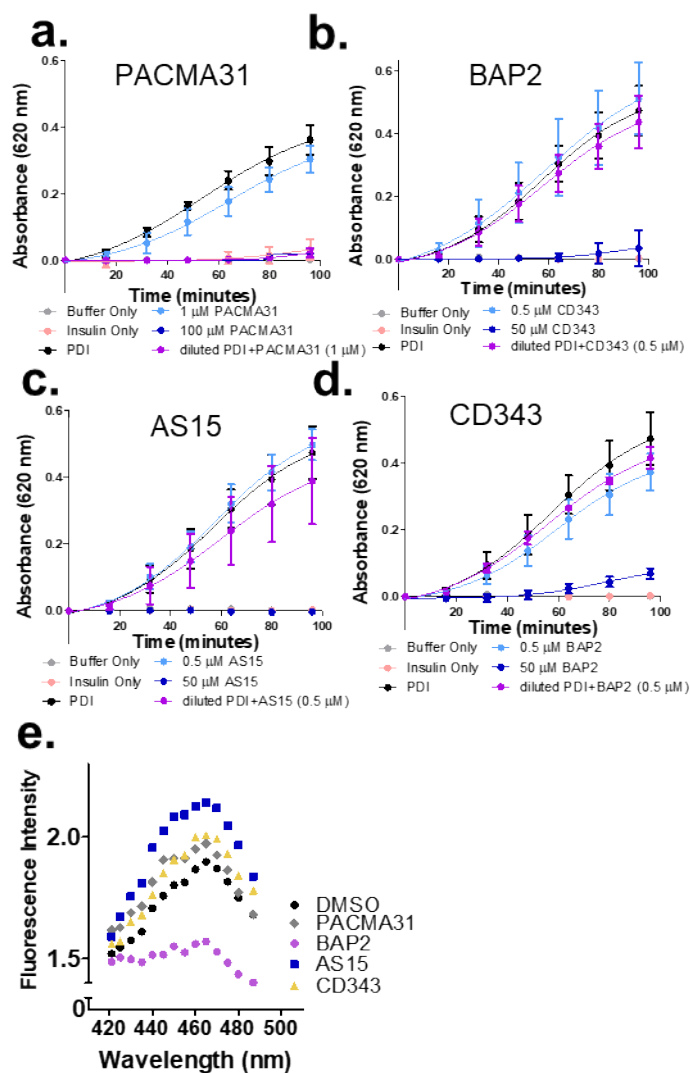
addition reaction. (d) **6a** covalently binds to PDI. 100 μM **6a** was incubated with 10 μM PDI and 100 μM

DTT for 30 min prior to injection. (e) **6a** binds to PDI preferentially over GSTO1. 100 μM **6a** was incubated

1
2
3 with a mixture of 10 μ M PDI, 10 μ M GSTO1, and 10 μ M GRP78 as a non-specific binding control for 30 min
4
5
6 prior to injection. (Close-up of GRP78 trace in Supplementary Figure S3.) (f) Concentration- and
7
8
9 time-dependent PDI inhibition curves for $k_{\text{inact}}/K_{\text{I}}$ determination of **PACMA31**, **16F16**, and **AS15**. Activity
10
11
12 was measured using the PDI reductase assay. Absorbance was monitored over time at various
13
14
15 concentrations and preincubation times with indicated compounds. (g) Gel-based competition with
16
17
18 recombinant PDI, PDI inhibitors or inactive analogue **6f** at 100 μ M, and **PACMA57**.
19
20
21
22
23

24 To address whether the **AS15** analogues targeted PDI irreversibly, like **PACMA31**, we
25
26 performed washout experiments with the PDI reductase assay. **AS15** (50 μ M) was incubated with
27
28 40 μ M PDI for 3 hours at room temperature. After 3 hours, the PDI-**AS15** complex was diluted
29
30 100-fold into reaction buffer, the reaction was incubated another hour at 37 $^{\circ}$ C, and insulin was
31
32 added as a substrate to initiate the reaction. **PACMA31** (an irreversible inhibitor) at 1 and 100 μ M
33
34 (**Figure 4A**) and **BAP2** (a reversible inhibitor) at 0.5 and 50 μ M (**Figure 4B**) were used as controls.
35
36 We found that both **AS15** and **CD343** did not maintain the characteristics of the high concentration
37
38 of inhibitor after dilution to the low concentration (**Figures 4C-D**). However, when we tested
39
40 enzyme activity recovery with compound concentrations 10 times that of the protein to mimic the
41
42 mass spectrometry conditions, **AS15** behave like the expected irreversible inhibitor (**Figure S4**).
43
44
45 **CD343** and **6a** were too active at this ratio. We further tested whether the compounds were binding
46
47 in the **b'** domain of oxidized PDI with the ANS (anilinonaphthalene sulfonic acid) spectral scan.³²
48
49 ANS is a dye that fluoresces upon binding hydrophobic pockets and specifically targets the **b'**
50
51 domain in PDI. **B'** domain-selective inhibitors of PDI such as estradiol and bepristat 1a compete
52
53 with ANS.³² **AS15** and **CD343** did not lower the fluorescence of ANS (**Figure 4E**). Our combined
54
55
56
57
58
59
60

1
2
3 results from the thermal shift assay, washout experiment, and ANS spectral scan demonstrated that
4
5 **AS15** and **CD343** are likely not substrate-binding domain inhibitors like estradiol and **BAP2**, but
6
7 may be covalent inhibitors of PDI.
8
9



10
11
12
13
14
15
16
17
18
19
20
21
22
23
24
25
26
27
28
29
30
31
32
33
34
35
36
37
38
39
40
41
42
43
44
45
46
47
48
49
50 **Figure 4.** Recovery of PDI activity upon treatment with **PACMA31** (a), **BAP2** (b), **AS15** (c), or **CD343** (d).

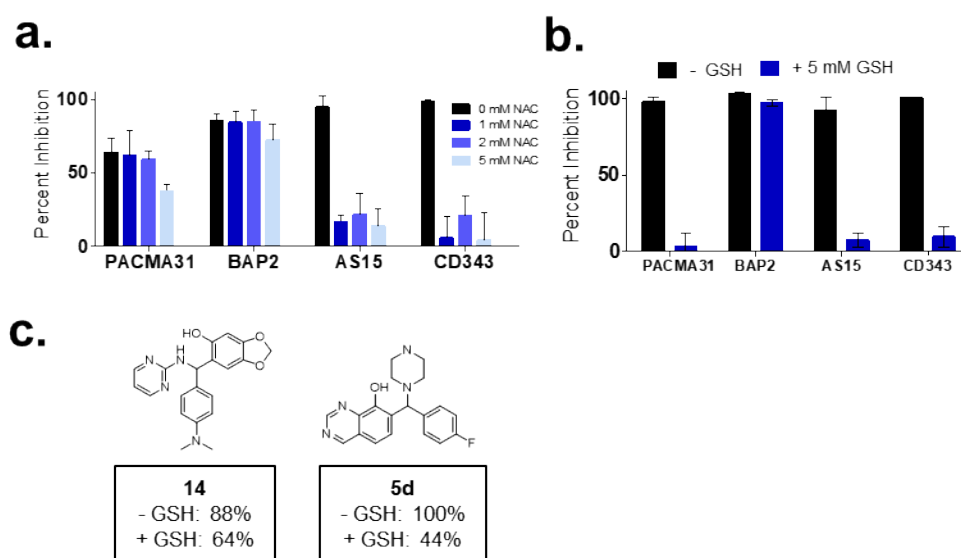
51
52
53 For the diluted samples (purple curves), 40 μM PDI was incubated with 100 μM **PACMA31**, 50 μM **BAP2**,

1
2
3 50 μ M **AS15**, or 50 μ M **CD343** for 3 h at rt before dilution. (f) ANS spectral scan with 5 μ M PDI and 100 μ M
4
5
6 **PACMA31**, **BAP2**, **AS15**, or **CD343**.
7
8
9

10
11
12
13 **AS15 Analogues Compete with Glutathione.** Because the **AS15** analogues seemed highly
14
15 reactive toward nucleophilic attack, we hypothesized that glutathione may also react with the
16
17 compounds. Glutathione is present in high concentrations in the cytoplasm and is an important
18
19 redox regulator in the ER.³³ The oxidizing environment of the ER is maintained by the ratio of
20
21 reduced to oxidized glutathione, which is lower than the ratio in the cytoplasm. Incubating the
22
23 compounds with N-acetyl cysteine (NAC) before adding them to the PDI reductase assay rendered
24
25 the compounds inactive (**Figure 5A**). Although both the **AS15** series and **PACMA31** are
26
27 irreversible PDI inhibitors, the differing characteristics in the NAC competition assay, as well as
28
29 differing kinetics, suggest that the compounds may have different mechanisms of action. **AS15**
30
31 analogues were also inactivated with competing glutathione at physiological concentrations (5
32
33 mM) in the PDI reductase assay (**Figure 5B**). The compounds retained activity when incubated
34
35 with PDI before adding GSH or NAC, providing further evidence of potential thiol reactivity
36
37 (**Figure S5**).
38
39
40
41
42
43

44 To assess trends in the glutathione sensitivity of the **AS15** series, we screened all the
45
46 analogues in the PDI reductase assay in the presence of 5 mM GSH. The high concentrations of
47
48 glutathione in the cytoplasm may inactivate the compounds *in vivo*; thus, the *in vitro* IC₅₀ value
49
50 may not be a reliable indicator of *in vivo* activity.¹⁴ Although the PDI reductase assay is performed
51
52 at a relatively high concentration of DTT (500 μ M), we added 5 mM glutathione to mimic a more
53
54 physiological environment (**Table S2**). This issue is particularly relevant because the analogues
55
56
57
58
59
60

1
2
3 behave as reversible thiol adducts. Substrate-binding domain inhibitors isoquercetin and **BAP2**
4 remained active in the presence of high GSH concentrations. Most of the **AS15** analogues were
5 remained active in the presence of high GSH concentrations. Most of the **AS15** analogues were
6 inactive in the presence of competing GSH. These results provided further support that the **AS15**
7 inactive in the presence of competing GSH. These results provided further support that the **AS15**
8 analogues may act *via* addition to PDI. We found two **AS15** analogues that maintained potency in
9 the presence of competing glutathione: **14** and **5d** (Figure 5C).
10
11
12
13
14
15
16
17
18
19



28
29
30
31
32
33
34
35
36
37
38 **Figure 5.** N-Acetyl cysteine and glutathione inactivate **AS15** analogues. (a) N-Acetyl cysteine (NAC)
39 competition in PDI reductase assay. Compounds were incubated with NAC prior to addition to a final
40 concentration of 10 μ M in the PDI reductase assay with PDIA1. (b) Glutathione competition in PDI reductase
41 assay. GSH was added to the PDI reaction buffer prior to 10 μ M compound addition. (c) Top two **AS15**
42 analogues that are least sensitive to competition with 5 mM GSH in the PDI reductase assay.
43
44
45
46
47
48
49
50
51
52
53
54
55
56
57
58
59
60

1
2
3 After our GSH screen, we retested the purity of **14** and **5d** and observed that **5d**
4 spontaneously formed a dimer after long-term storage. As a result, we re-purified the monomeric
5 and dimeric forms of **5d** and tested each form in the PDI reductase assay in the presence of
6 glutathione (**Figure 6A**). The dimeric form of **5d** was less sensitive to glutathione competition
7 than the monomer (**Figure 6B**). Furthermore, we found that both the monomer and dimer of **5d**
8 bound to PDI (**Figure 6C**). Incubation with the a'c domain gave a species with two fragments of
9 **5d** monomer bound (**Figure S6A**). When we incubated the monomer and dimer of **5d** with a C53S
10 mutant of PDI, we observed one and two species bound, respectively (**Figure S6B**).
11
12
13
14
15
16
17
18
19
20
21

22 Although the PDI disulfides are 500-fold more reactive than glutathione³⁴, we
23 hypothesized that glutathione may be inactivating the **AS15** analogues and contributing to lower
24 their potency in cells. Pretreatment of GBM cells with BSO for 24 hours before adding the
25 compounds increased potency in the colony formation assay (**Figure 6D–H, Figure S7**). While
26 the monomer of **5d** was more sensitive to BSO addition, the **5d** dimer was more potent and its
27 potency was not dependent on BSO addition. These results support the hypothesis that glutathione
28 depletion sensitizes GBM cells to PDI inhibition.
29
30
31
32
33
34
35
36
37
38
39
40
41
42
43
44
45
46
47
48
49
50
51
52
53
54
55
56
57
58
59
60

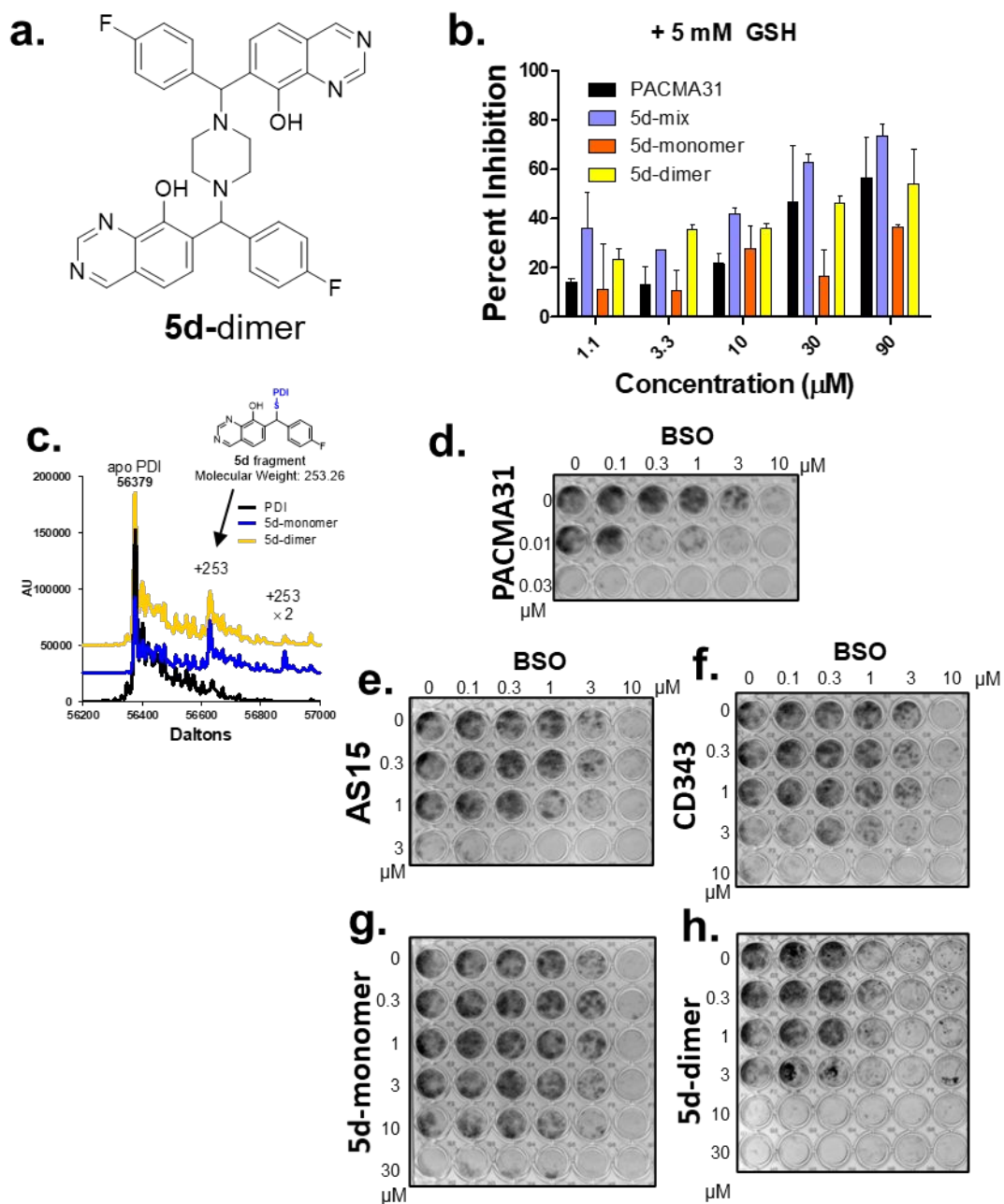


Figure 6. Dimerized analogue is less sensitive to GSH treatment. (a) Structure of **5d** dimerization. (b) Percent inhibition of **5d** monomer and dimer in the PDI reductase assay in competition with 5 mM glutathione. (c) Protein mass spectrometry confirms fragment of **5d** binds to PDI. Toxicity of **PACMA31** (d), **AS15** (e), **CD343** (f), **5d**

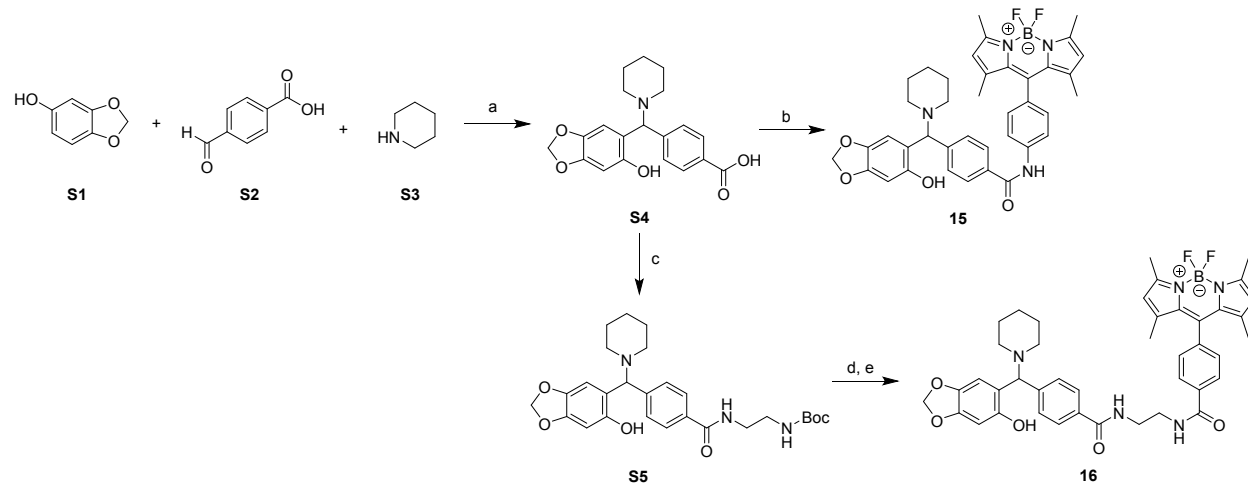
1
2
3 monomer (g), and **5d** dimer (h) in the colony formation assay in the absence or presence of BSO. U-118 MG cells
4
5 were pretreated with BSO for 24 h prior to compound addition.
6
7
8
9

10 **AS15 Analogue Target Identification.** We sought to confirm whether the **AS15** analogues could
11 target PDI in the cells by synthesizing two analogues of **6b** with a BODIPY fluorescent tag on the
12 phenyl ring (**Scheme 4, Figure 7A**). The BODIPY-labeled compounds differed in the linker
13 length between the parent compound and the tag. One compound was directly attached to BODIPY
14 with an amide linkage on the phenyl ring (**15**), while the other (**16**) contained a two-carbon linker
15 separating the amide groups on the BODIPY structure. **15** did not inhibit PDI activity in the PDI
16 reductase assay (**Figure S8**). However, it did covalently bind proteins around 55–70 kDa when
17 added to cells (**Figure 7B**). This prompted us to perform in-gel digestion and mass spectrometry
18 of the proteins at this size (**Table 8**). Albumin, the most abundant plasma protein, was identified
19 as one of the proteins in the band, and incubation of both **15** and **16** with cell-free medium
20 supplemented with fetal bovine serum demonstrated that the compounds bound to serum albumin
21 (**Figure 7C**). Although **16** bound to serum albumin, it inhibited PDI activity with an IC_{50} value
22 comparable to the parent compound of $1.37 \pm 0.23 \mu\text{M}$ (**Figure 7D**). To verify the band from **15**
23 was not PDI, a Western blot was performed with cells treated with **15** and **16**. The GFP band from
24 the **15**-treated cells runs closer to the molecular weight of albumin (69 kDa) than the PDI band
25 around 55 kDa (**Figure S9A**). Additionally, when the cells were treated with **15** after serum
26 starvation, the band disappeared (**Figure S9B**). With recombinant PDI, **16** covalently binds, and
27 binding can be blocked with DTT, further supporting the mechanism of inhibition of this series
28 (**Figure S10**).
29
30
31
32
33
34
35
36
37
38
39
40
41
42
43
44
45
46
47
48
49
50
51
52
53
54
55
56
57
58
59
60

1
2
3
4
5
6
7
8
9
10
11
12
13
14
15
16
17
18
19
20
21
22
23
24
25
26
27
28
29
30
31
32
33
34
35
36
37
38
39
40
41
42
43
44
45
46
47
48
49
50
51
52
53
54
55
56
57
58
59
60

Table 8. Most Abundant Proteins around 55–70 kDa in U-118 MG Cells

accession	description	# cysteines	location	coverage [%]	# peptides	# PSMs	# unique peptides	MW [kDa]
P14618	Pyruvate kinase PKM (PKM)	10	nucleus	70	33	181	33	57.9
P10809	60 kDa heat shock protein, mitochondrial (HSPD1)	3	mitochondria	72	34	104	34	61
P07237	Protein disulfide-isomerase (P4HB)	7	ER/membrane	70	31	70	31	57.1
P31948	Stress-induced-phosphoprotein 1 (STIP1)	11	nucleus	57	29	63	29	62.6
P48643	T-complex protein 1 subunit epsilon (CCT5)	8	cytoplasm	68	30	62	29	59.6
P17987	T-complex protein 1 subunit alpha (TCP1)	9	cytoplasm	68	27	57	27	60.3
Q16555	Dihydropyrimidinase-related protein 2 (DPYSL)	8	cytoplasm	70	27	57	24	62.3
P49368	T-complex protein 1 subunit gamma (CCT)	10	cytoplasm	69	31	56	31	60.5
P02768	Serum albumin (ALB)	35	extracellular	12	7	55	7	69.3
P30153	Serine/threonine-protein phosphatase 2A 65 kDa regulatory subunit A alpha isoform (PPP2R1A)	14	nucleus	60	27	47	20	65.3
P61978	Heterogeneous nuclear ribonucleoprotein K (HNRNPK)	5	nucleus	56	20	46	20	50.9
P50990	T-complex protein 1 subunit theta (CCT8)	10	cytoplasm	56	28	45	28	59.6
P54577	Tyrosine-tRNA ligase, cytoplasmic (YARS)	6	cytoplasm	60	28	38	28	59.1
O43242	26S proteasome non-ATPase regulatory subunit 3 (PSMD3)	2	extracellular, nucleus, cytoplasm	51	24	36	24	60.9
O75083	WD repeat-containing protein 1 (WDR1)	12	cytoskeleton	53	21	35	21	66.2
P36871	Phosphoglucosyltransferase-1 (PGM1)	5	extracellular, cytoplasm	55	23	34	23	61.4
Q99832	T-complex protein 1 subunit eta (CCT7)	9	cytoplasm	55	22	32	22	59.3
P02545	Prelamin-A/C (LMNA)	5	nucleus	36	25	32	25	74.1
P40227	T-complex protein 1 subunit zeta (CCT6A)	8	cytoplasm	56	21	32	21	58
Q9H4M9	EH domain-containing protein 1 (EHD1)	1	membrane, endosome	58	21	31	21	60.6
O43776	Asparagine-tRNA ligase, cytoplasmic (NARS)	15	cytoplasm	38	18	30	18	62.9
P29401	Transketolase (TKT)	12	extracellular, nucleus, cytoplasm	43	17	28	17	67.8
P68363	Tubulin alpha-1B chain (TUBA1B)	12	cytoskeleton	65	19	28	2	50.1

Scheme 4. Synthetic route for compounds **15** and **16**.^a

^aReagents and conditions: a) toluene, 100 °C; b) 4-(5,5-difluoro-1,3,7,9-tetramethyl-5H-4λ⁴,5λ⁴-dipyrrolo[1,2-*c*:2',1'-*f*][1,3,2]diazaborinin-10-yl)aniline (BODIPY aniline), EDCI, HOBt, DMF, rt; c) *tert*-butyl (2-aminoethyl)carbamate, HATU, DIEA, DMF, rt; d) TFA, DCM, rt; e) 4-(5,5-difluoro-1,3,7,9-tetramethyl-5H-4λ⁴,5λ⁴-dipyrrolo[1,2-*c*:2',1'-*f*][1,3,2]diazaborinin-10-yl)benzoic acid, HATU, DIEA, DMF, rt.

To further investigate whether the BODIPY-labeled **AS15** analogues target PDI, we treated cell lysates with the compounds for 24 hours. **15** did not covalently label proteins in the cell lysate; however, **16** bound in two major bands around 55 and 40 kDa, and a minor band below 55 kDa (**Figure 7E**, **Figure S11**). In addition, the parent compound competed for labeling both bands in a dose-dependent manner but seemed to compete off the 55 kDa band at a lower concentration (5x [probe]) than the 40 kDa band (20x [probe]) (**Figure 7F**). In addition to inhibiting PDIA1 activity, **AS15** could also inhibit PDIA3 activity; thus, the band around 55 kDa could contain both PDIA1 and PDIA3. Compound **16** bound PDIA1, PDIA2, and PDIA3, in

1
2
3 addition to BSA, and was competed off by the parent compound. Competition was not observed
4
5 for binding to BSA, likely due to multiple binding sites for **16** on BSA (**Figure S12**). **6b**
6
7 dose-dependently competed off **16** for binding PDIA2 and PDIA3 (**Figure S13**). Combining BSA
8
9 with PDIA1 for 24 hours with **15** or **16** did not improve binding to PDIA1 (**Figure S14**). Because
10
11 glutathione inactivated the compounds *in vitro*, cells were pre-incubated with BSO prior to
12
13 BODIPY-labeled compound treatment to determine whether depleting the cells of glutathione
14
15 would improve on-target binding. BSO addition improved binding for **15**, however, binding was
16
17 non-selective. Furthermore, addition of 10% FBS decreased binding, further confirming the
18
19 interaction between this series and serum albumin (**Figure S15A**).
20
21
22
23
24
25
26
27
28
29
30
31
32
33
34
35
36
37
38
39
40
41
42
43
44
45
46
47
48
49
50
51
52
53
54
55
56
57
58
59
60

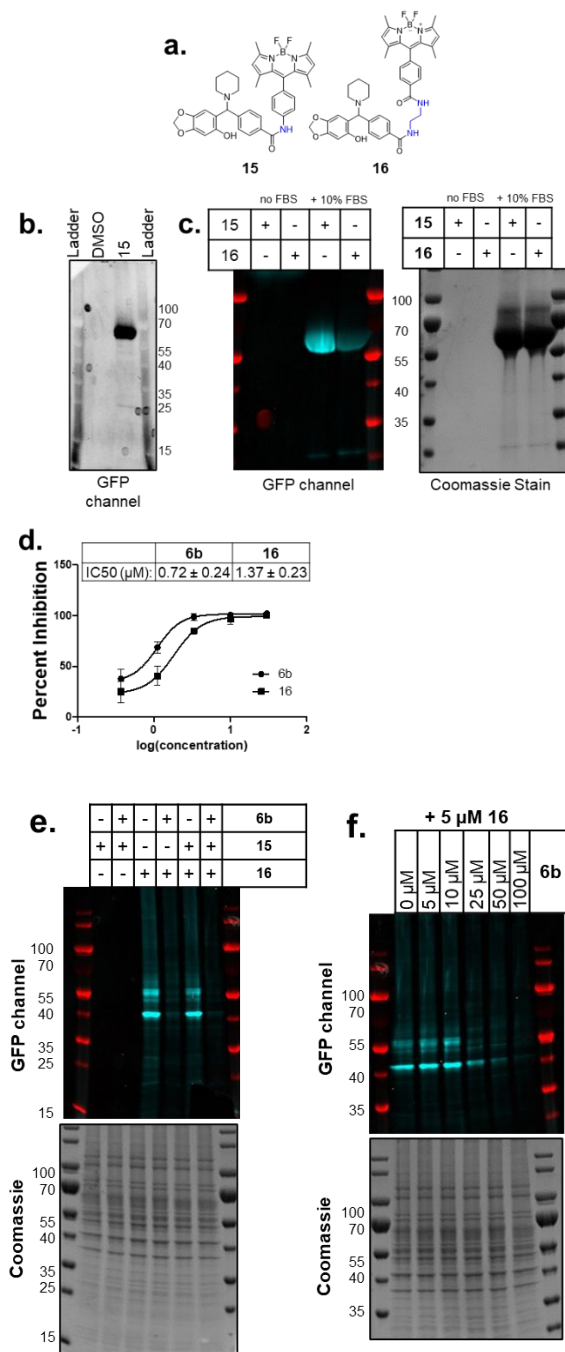
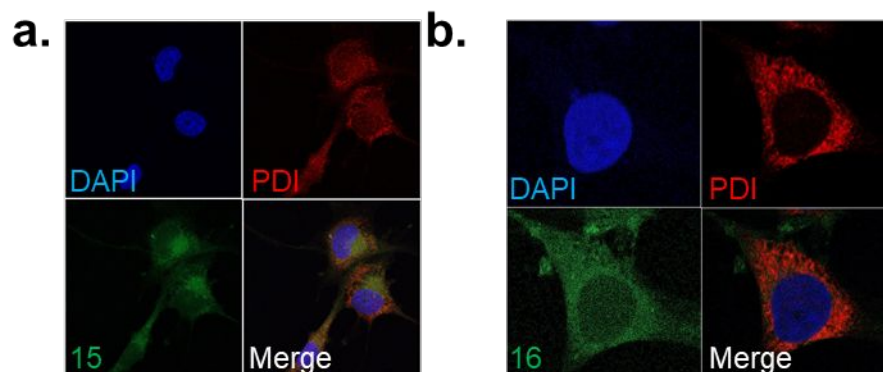


Figure 7. AS15 analogues bind serum albumin. (a) Structures of BODIPY-labeled AS15 analogues (b) U-118 MG cells treated with 40 μM 15 overnight (c) Cell-free DMEM treated with 20 μM 15 or 16 overnight at 37 °C. (d) 16 dose-response curve in the PDI reductase assay. (e) Cell lysates incubated with 50 μM 6b

1
2
3 and 5 μM **15** or **16** for 24 h at room temperature after cell lysis. (f) Cell lysates treated with increasing
4
5
6 concentrations of parent compound **6b** before addition of BODIPY-labeled **16**.
7
8
9
10
11

12 Incubation of the cell lysate with **16** consistently resulted in multiple bands (**Figure S16B**).
13
14 Proteomic analysis of each of the bands revealed PDIA1 among other targets in the cell lysate
15
16 (**Table S3–S4; Supplemental File 1**). Because of the reactivity of these compounds, it is possible
17
18 that they bind to proteins besides PDIA1 in the cell lysate. Reported targets of similar scaffolds
19
20 include MIF tautomerase, HDAC5/9, and BRAF^{V600E}. However, we did not observe bands at the
21
22 molecular weights of those three targets, suggesting the **AS15** analogues do not bind these proteins,
23
24 or the proteins have low abundance in the cell lines tested. Furthermore, those known targets, as
25
26 well as STAT3, STAT5, Mcl-1, frataxin, and P2Y12, were not found in the bands analyzed with
27
28 the proteomics experiment. In addition, confocal microscopy revealed that the BODIPY-labeled
29
30 analogues mainly reside in the cytoplasm and ER, not in the nucleus with HDAC5/9 and BRAF
31
32 (**Figure 8**).
33
34
35
36
37
38



1
2
3 **Figure 8.** Confocal microscopy images at 60X magnification of A-172 cells treated with 10 μ M **15** (a) or 2
4
5
6 μ M **16** (b) for 24 h prior to fixation and staining for PDI.
7
8
9

10
11
12
13
14
15 **AS15 Analogue Activates the Unfolded Protein Response.** We performed nascent RNA
16
17
18
19 sequencing of one of the most potent analogues of **AS15**, **5p**, to analyze changes in gene
20
21
22 transcription in U-87 MG cells (**Figure 9A**).³⁵ Four hours after 20 μ M **5p** treatment, 68
23
24
25
26 genes were upregulated at least two-fold and 12 genes were downregulated at least
27
28
29 two-fold (**Tables S5-S12; Supplemental File 2**). We performed Gene Set Enrichment
30
31
32
33 Analysis on the pre-ranked gene list of 7907 genes and identified that **5p** upregulates
34
35
36 transcription of genes involved in the unfolded protein response (**Figure 9B, Figure S16**).
37
38 STRING (Search Tool for the Retrieval of Interacting Genes/Proteins) interactions of significant
39
40
41 genes in the **5p** Bru-seq dataset also demonstrated genes affected were involved in protein folding,
42
43 ER stress, and response to ER stress (**Figure 9C, Table S13**). Affected UPR genes included *CALR*
44
45 (**Figure 9D**), *HSPA5* (**Figure 9E**), *MYZAP* (**Figure 9F**), *NQO1* (**Figure 9G**), and *SLC7A11*
46
47 (**Figure 9H**). Calreticulin (*CALR*) is an ER chaperone like PDI, specifically folds glycoproteins to
48
49 be secreted, and mediates calcium homeostasis in the organelle.³⁶ Calreticulin acts as a sensor of
50
51 ER stress because ER Ca^{2+} depletion triggers ER stress. Calreticulin has been demonstrated to bind
52
53 to ERp57 and regulate glycoprotein isomerization.³⁷ However, **5p** treatment did not increase total
54
55
56
57
58
59
60

1
2
3 cellular CALR expression in brain cancer cells (**Figure 9I**). *HSPA5* encodes for GRP78/BiP, an
4 important chaperone responsible for promoting tumor growth.³⁸ Nascent polypeptides enter the
5 ER and interact with GRP78/BiP to initiate protein folding. Increased transcription of GRP78/BiP
6 indicates the cells are undergoing an unfolded protein stress response. NAD(P)H Quinone
7 Dehydrogenase 1 (*NQO1*) is a cytosolic quinone reductase that promotes quinone–glutathione
8 conjugation and removal from the cells. It is generally highly expressed in cancers and allows the
9 tumor to cope with increased cytotoxic stress.³⁹ *SLC7A11* encodes for a cystine/glutamate
10 antiporter protein that resides on the cell membrane. SLC7A11 is part of the system x_c^- antiporter
11 system that uptakes extracellular cystine as a precursor for GSH biosynthesis in exchange for
12 glutamate.⁴⁰ Interestingly, we observed upregulated transcription of *SLC7A11* upon treatment with
13 PDI inhibitor **35G8** as well.⁴¹ Our results indicate that PDI inhibition may be synthetically lethal
14 with system x_c^- inhibition. Myocardial zonula adherens (*MYZAP*) is part of a transcriptional unit
15 containing downstream gene *POLR2M* (polymerase (RNA) II (DNA directed) polypeptide M).
16 MYZAP protein is expressed in cardiac tissue and is involved in signaling via Rho–related
17 GTP–binding proteins. The Bru–seq RNA sequencing genes affected support **5p**–mediated PDI
18 inhibition in U–87 MG cells.
19
20
21
22
23
24
25
26
27
28
29
30
31
32
33
34
35
36
37
38
39
40
41
42
43
44
45
46
47
48
49
50
51
52
53
54
55
56
57
58
59
60

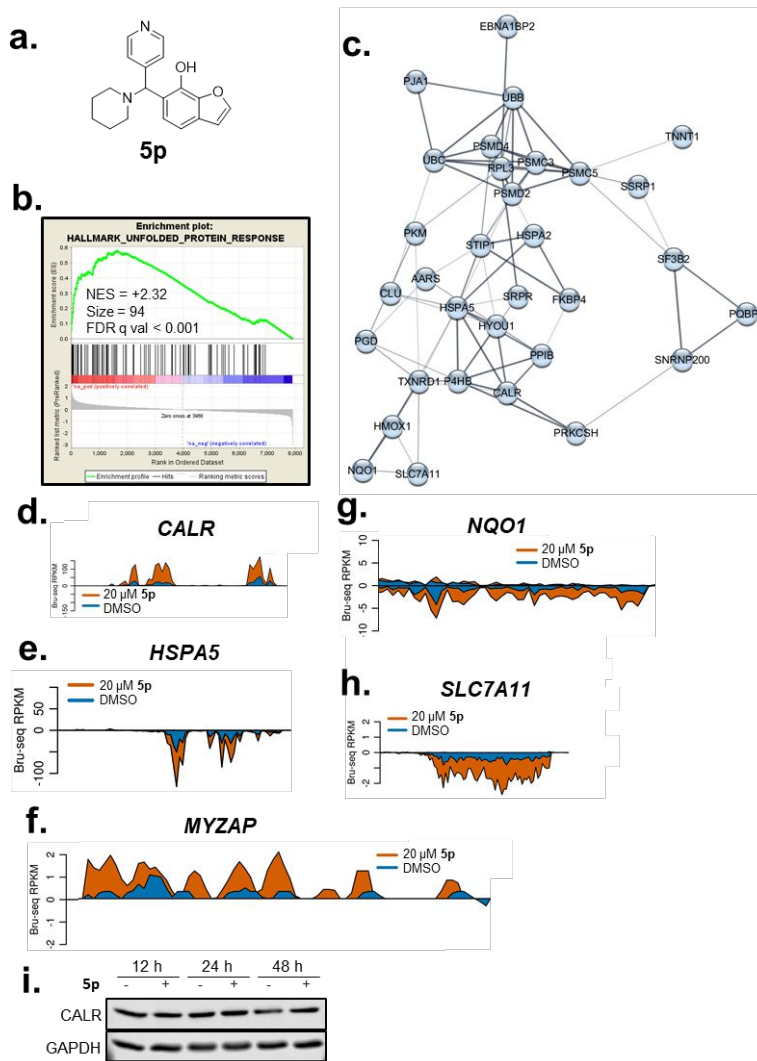


Figure 9. **5p** upregulates transcription of genes involved in the unfolded protein response. (a) Structure of **5p**. (b) **5p** promoted gene set enrichment related to the unfolded protein response. NES: normalized enrichment score. FDR q val: false discovery rate q value. Criteria for GSEA was $p < 0.05$ and false discovery rate < 25%. (c) STRING interactions of significant genes in **5p** Bru-seq dataset. Four-hour treatment with **5p** increases transcription of representative unfolded protein response genes including *CALR* (d), *HSPA5* (e), *MYZAP* (f), *NQO1* (g), and *SLC7A11* (h). (i) U-118 MG cells were treated with 20 μ M **5p** for 12, 24, or 48 h and probed for calreticulin protein expression. GAPDH is used as a loading control.

1
2
3 We further analyzed the Bru-seq signature of **5p** with the Connectivity Map (**Tables**
4 **S14–S20**).⁴² Because less than ten genes were significantly downregulated upon **5p** treatment, the
5 Connectivity Map analysis included only upregulated genes. **5p** had a similar gene expression
6 signature as the seleno-organic glutathione peroxidase mimetic ebselen.⁴³ Ebselen is an
7 antioxidant that is known to react with cysteines, and it targets GTPase protein Rac1 in
8 humans.^{44, 45} Interestingly, ebselen inhibits MIF tautomerase activity as well.²² This
9 indicates that the signature of **5p** may be an artifact of global cysteine reactivity rather
10 than selective target inhibition. Furthermore, the signature of **5p** demonstrated similarity with
11 knockdown of *KDEL3* (KDEL endoplasmic reticulum protein retention receptor 3). *KDEL3*
12 contains four cysteines and is upregulated as part of the unfolded protein response.⁴⁶ The protein
13 is in a family of three KDEL receptors localized to the ER and Golgi complex. These results
14 confirm that **5p** exhibits a cysteine-reactive signature in brain cancer cells.

DISCUSSION

15
16
17
18
19
20
21
22
23
24
25
26
27
28
29
30
31
32
33
34
35
36
37
38
39
40
41 Target engagement in cells is a critical aspect of preclinical targeted drug development. It
42 is important to understand and verify that the compound can reach the target, and that the
43 interaction causes the observed phenotype. There are multiple techniques used to assess target
44 engagement, including direct assays such as the cellular thermal shift assay (CETSA), drug affinity
45 responsive target stability (DARTS), the NanoLuc thermal shift assay, and bioluminescence
46 resonance energy transfer (BRET), or indirect methods such as knockdown effects or biomarker
47 expression.⁴⁷ In order to determine on-target labeling of PDI in cells, we synthesized two
48
49
50
51
52
53
54
55
56
57
58
59
60

1
2
3 variations of BODIPY–labeled **AS15** analogues. Our initial discovery upon treating cells with
4 these compounds was that the compounds bind to serum albumin, an abundant protein containing
5 35 cysteine residues. When the **AS15** analogues were incubated with the cell lysates, we observed
6 binding in three major bands, indicating that the compounds bound to proteins around 57 and 40
7 kDa. While plasma protein binding is a consideration for improvement of potency of this series,
8 proteomics analysis demonstrated that the BODIPY–labeled **AS15** analogues reach and bind
9 covalently to PDIA1 in the cells. Several PDI family members have a molecular weight around 40
10 kDa, including ERp44, PDIA6, and TXNDC5, which could be responsible for the lower band
11
12
13
14
15
16
17
18
19
20
21
22 **(Table 9)**.
23
24

25 **Table 9.** PDI Family Members and Molecular Weights

26

gene name	size (kDa)	gene name	size (kDa)
P4HB	55	PDIA12 (TMX2)	34
PDIA2	55	PDIA13 (TMX3)	52
PDIA3 (ERp57)	54	PDIA14 (TMX4)	39
PDIA4 (ERp72)	71	(TMX5)	not reported
PDIA5 (PDIR)	57	PDIA15 (ERp46)	48
PDIA6 (P5)	46	PDIA16 (ERp19, AGR1)	18
PDIA7 (PDILT)	67	PDIA17 (AGR2, HAG–2)	20
PDIA8 (ERp27)	30	PDIA18 (AGR3, HAG–3)	19
PDIA9 (ERp29)	29	PDIA19 (ERdj5)	91
PDIA10 (ERp44)	44	PDIB1 (CASQ1)	45
PDIA11 (TMX1)	32	PDIB2 (CASQ2)	46

27
28
29
30
31
32
33
34
35
36
37
38
39
40
41
42
43
44
45
46
47
48
49
50
51
52
53
54
55
56
57
58
59
60

1
2
3 These results corroborate previous findings with this Mannich base series. Targets
4 identified for this series of compounds are summarized in **Table S21**. The frataxin inhibitor, which
5 differs from **AS15** by only an ortho methoxy in place of the para methoxy, was non-toxic up to
6 100 μM in cells and dose-dependently prevented the ubiquitination of frataxin. The authors did
7 not perform selectivity experiments since they were measuring a cellular protein function;
8 however, they did show that the compound did not bind denatured protein. In the same year,
9 another group reported a series of hydroxyquinolines similar to **CD343** as selective Mcl-1
10 inhibitors. With an SAR campaign, they demonstrated that the hydroxyl group and nitrogen were
11 important for Mcl-1 activity. While we did not test their reported Compound 9, **5a** and **5b** were
12 similar compounds, with the piperazine replaced by a morpholino group or pyrazine group. These
13 compounds had submicromolar IC_{50} values in the PDI reductase assay, similar to the IC_{50} value
14 against Mcl-1 in the fluorescence polarization assay.⁴⁸ In terms of selectivity, the researchers were
15 able to demonstrate a correlation between a downstream response to Mcl-1 inhibition, cytochrome
16 c release, and the extent of mitochondrial priming in cells.⁴⁸ Further targets of this series include
17 HDAC5/9, STAT3/5, BRAF^{V600E}, and P2Y12. **NC124** was highly potent against leukemia cell
18 lines (THP-1 and KASUMI-1), though it was much less potent against U-87 MG cells ($\text{IC}_{50} =$
19 $24.2 \pm 7.1 \mu\text{M}$), possibly because TET1 expression is relatively lower in the U-87 MG cells.⁴⁹
20 Interestingly, several groups reported that this series of compounds passed protein reactivity filters.
21
22
23
24
25
26
27
28
29
30
31
32
33
34
35
36
37
38
39
40
41
42
43
44

45 Because the analogues we tested were inactivated by GSH addition in the PDI reductase
46 assay, we tested whether GSH depletion in a cell-based assay would influence potency. The
47 compounds were more potent when cells were treated with non-toxic concentrations of BSO, the
48 glutathione synthesis inhibitor. This result suggests that either the compounds are being
49 sequestered by GSH in the cytoplasm and unable to reach the target protein, or that GSH depletion
50
51
52
53
54
55
56
57
58
59
60

1
2
3 prevents PDI from rescue. Thus, a potential strategy for further modification would include
4
5 decreasing GSH reactivity of the series. The glutathione-mediated antioxidant defense
6
7
8
9 system is upregulated in cancer cells compared to normal cells to mitigate the harmful
10
11
12 byproducts of increased cell metabolism.⁵⁰ Increased concentrations of GSH are
13
14
15 responsible for resistance to anti-cancer therapy. Temozolomide-resistant GBM tumors
16
17
18
19 rely on glutathione antioxidant signaling pathways for survival.⁵¹ Glutathione promotes
20
21
22 metastasis in liver cancer, and overexpression of glutathione synthesis enzymes has
23
24
25
26 been linked with drug resistance.^{52, 53} Thus, glutathione depletion, in particular with the
27
28
29
30 irreversible glutamate cysteine ligase (GCL) inhibitor buthionine sulfoximine (BSO), may
31
32
33
34 be a promising combinatorial approach with this series. Additionally, it should be noted
35
36
37 that PDI is present in a mixed population in the cells under physiological conditions.
38
39
40
41 Therefore, cell-based experiments have been performed with the endogenous population
42
43
44 of PDI.

48 CONCLUSIONS

51 Starting from a lead compound containing a benzobenzoxole scaffold and
52
53
54
55 morpholine moiety, we investigated modifications around the core. The trends in the
56
57

1
2
3 structure–activity relationships of the analogues that a tertiary amine and hydroxyl group
4
5
6
7 were critical for activity suggest that the potency of the inhibitors likely relies on the thiol-
8
9
10 reactive characteristics. Protein mass spectrometry analysis further identified that **AS15**
11
12
13 analogues bound covalently to PDI after displacement of the amine group. Though the
14
15
16
17 compounds were potent *in vitro* inhibitors of PDI, glutathione inactivated the compounds,
18
19
20 and BODIPY–labeled analogues bound serum albumin. Because of the binding pattern of the
21
22
23
24 **AS15** analogues and reactivity with glutathione, they have the potential to be optimized
25
26
27 as *in vivo* thiol–reactive inhibitors. Notably, this study is the first to explore the reactivity and
28
29
30 regioselectivity of a variety of hydroxy bicyclic heterocycles in Betti-style reactions and the
31
32
33 biological activity of their products. Furthermore, our in-depth mechanistic studies demonstrate
34
35
36 their mechanism of action is directly related to PDI inhibition.
37
38

39 **EXPERIMENTAL SECTION**

40
41 **General Methods.** All commercial reagents and anhydrous solvents were purchased and used
42
43 without purification, unless specified. Column chromatography was performed on a Biotage
44
45 Isolera flash chromatography system on Biotage normal phase Silica Gel columns. Analytical thin
46
47 layer chromatography was performed on Merck pre–coated plates (Silica Gel 60 F₂₅₄). NMR
48
49 spectra were recorded on a Bruker Ultrashield 300 MHz or Bruker Ascend 400 MHz spectrometer
50
51 using deuterated CDCl₃ or CD₃OD as solvents. Chemical shifts for proton magnetic resonance
52
53 spectra (¹H NMR) are listed in parts per million (ppm) referenced to the appropriate solvent peak
54
55
56
57
58
59
60

1
2
3 or 0.0 ppm for tetramethylsilane (TMS). The following abbreviations are used to describe the
4 peak-splitting patterns when appropriate: br, broad; s, singlet; d, doublet; t, triplet; q, quartet; m,
5 multiplet; and dd, doublet of doublets. Coupling constants, J, are reported in hertz (Hz). Mass
6 spectra were recorded on a Shimadzu LCMS-2020 system using the electro spray ionization (ESI)
7 ion source. HPLC was used to determine the purity of biologically tested compounds using
8 Shimadzu LC-2030C 3D system on Kinetex XB-C18 column (2.6 μm , 4.6 \times 75 mm) under the
9 following gradient elution conditions: acetonitrile/water (10–95%) or methanol/water (10–95%).
10 The purity was established by integration of the areas of major peaks detected at 254 nm, and all
11 tested compounds including the **NC** and **CD** series compounds have >95% purity.
12
13
14
15
16
17
18
19
20
21
22
23

24 **General Synthesis Procedure A.**

25 Phenolic compound, amine, and aldehyde were dissolved in toluene. The mixture was heated at
26 100 °C for specified time and monitored by TLC. After completion of the reaction, the mixture
27 was concentrated, and the residue was purified by flash chromatography to give the target
28 compound.
29
30
31
32
33
34

35 **General Synthesis Procedure B.**

36 Phenolic compound, amine, and aldehyde were dissolved in EtOH. The mixture was heated at 120
37 °C for 0.5 h under microwave or refluxed overnight. After completion of the reaction, the mixture
38 was concentrated, and the residue was purified by flash chromatography or recrystallized from
39 methanol/acetone to give the target compound.
40
41
42
43
44
45
46

47 **7-((2,3-Dimethoxyphenyl)(morpholino)methyl)quinolin-8-ol (5a).** Prepared from 2,3-
48 dimethoxybenzaldehyde, (85 mg, 0.51 mmol), 8-hydroxyquinoline (50 mg, 0.34 mmol), and
49 morpholine (44 mg, 0.51 mmol) in toluene at 100 °C overnight. After concentration, the residue
50 was purified by silica column chromatography (EtOAc : MeOH = 10:1) to give compound **5a** as a
51
52
53
54
55
56
57
58
59
60

1
2
3 pale yellow solid (16% yield). ¹H NMR (300 MHz, CDCl₃): 12.13 (s, 1H), 8.89 (dd, *J* = 4.2, 1.7
4 Hz, 1H), 8.05 (dd, *J* = 8.3, 1.7 Hz, 1H), 7.38 (dd, *J* = 8.3, 4.2 Hz, 1H), 7.35–7.18 (m, 4H), 6.99
5
6 (t, *J* = 8.0 Hz, 1H), 6.81 (dd, *J* = 8.2, 1.4 Hz, 1H), 5.33 (s, 1H), 3.94 (s, 3H), 3.87 (s, 4H), 3.86–
7
8 3.72 (m, 4H), 2.82–2.53 (m, 6H); MS (ESI) *m/z* = 381.2 [M + H]⁺. Purity 97.7%.

9
10
11 **7-((4-Fluorophenyl)(piperidin-1-yl)methyl)quinolin-8-ol (5b)**. Prepared from 4-
12
13 fluorobenzaldehyde (103 mg, 0.83 mmol), 8-hydroxyquinoline (80 mg, 0.55 mmol), and piperidine
14
15 (70 mg, 0.83 mmol) in toluene at 100 °C overnight. After concentration, the residue was purified
16
17 by silica column chromatography (DCM : EtOAc : NH₄OH = 5:1:0.1) to give compound **5b** as a
18
19 pale yellow solid (98 mg, 53% yield). ¹H NMR (300 MHz, CDCl₃): 12.82 (s, 1H), 8.90 (d, *J* = 4.1
20
21 Hz, 1H), 8.04 (d, *J* = 8.3 Hz, 1H), 7.47 (dd, *J* = 8.3, 5.3 Hz, 2H), 7.37 (dd, *J* = 8.3, 4.2 Hz, 1H),
22
23 7.18 (s, 2H), 6.98 (t, *J* = 8.5 Hz, 2H), 4.66 (s, 1H), 2.76–2.35 (m, 4H), 1.84–1.39 (m, 6H); MS
24
25 (ESI) *m/z* = 337.2 [M + H]⁺. Purity 96.6%.

26
27
28 **7-((4-Fluorophenyl)(piperidin-1-yl)methyl)quinazolin-8-ol (5c)**. Prepared from 4-
29
30 fluorobenzaldehyde (39 mg, 0.32 mmol), 8-hydroxyquinazoline (30 mg, 0.21 mmol), and
31
32 piperidine (27 mg, 0.32 mmol) in toluene at 100 °C overnight. After concentration, the residue was
33
34 purified by silica column chromatography (EtOAc : MeOH = 100:1) to give compound **5c** as a
35
36 white solid (30 mg, 42% yield). ¹H NMR (300 MHz, CDCl₃) δ 13.68 (s, 1H), 9.33 (s, 1H), 9.28 (s,
37
38 1H), 7.43 (t, *J* = 6.5 Hz, 2H), 7.32–7.18 (m, 2H), 7.01 (t, *J* = 8.5 Hz, 2H), 4.67 (s, 1H), 2.78–2.22
39
40 (s, 4H), 1.84–1.48 (m, 6H); MS (ESI) *m/z* = 338.5 [M + H]⁺. Purity 98.4%.

41
42
43 **7-((4-Fluorophenyl)(piperazin-1-yl)methyl)quinazolin-8-ol (5d)**. Prepared from 4-
44
45 fluorobenzaldehyde (51 mg, 0.41 mmol), 8-hydroxyquinazoline (40 mg, 0.28 mmol), and
46
47 piperazine (36 mg, 0.41 mmol) in toluene at 100 °C overnight. After concentration, the residue
48
49 was purified by silica column chromatography (EtOAc : MeOH = 100:1) to give compound **5d** as
50
51
52
53
54
55
56
57
58
59
60

1
2
3 a white solid (6 mg, 6% yield). ¹H NMR (300 MHz, CDCl₃) δ 9.31 (d, *J* = 6.2 Hz, 2H), 7.52–7.31
4 (m, 4H), 7.01 (t, *J* = 8.4 Hz, 2H), 4.76 (s, 1H), 3.07 (d, *J* = 11.5 Hz, 4H), 2.62 (d, *J* = 23.5 Hz, 4H);
5
6 MS (ESI) *m/z* = 339.0 [M + H]⁺. Purity 97.3%.
7
8

9
10 **6-((4-Fluorophenyl)(piperidin-1-yl)methyl)quinoxalin-5-ol (5e)**. Prepared from 4-
11 fluorobenzaldehyde (102 mg, 0.82 mmol), quinoxalin-5-ol (80 mg, 0.55 mmol), and piperidine
12 (71 mg, 0.82 mmol) in toluene at 100 °C overnight. After concentration, the residue was purified
13 by silica column chromatography (DCM : MeOH = 100:1) to give compound **5e** as a pale yellow
14 solid (46 mg, 25% yield). ¹H NMR (300 MHz, CDCl₃) δ 8.84–8.77 (m, 2H), 7.44 (q, *J* = 8.0, 7.0
15 Hz, 3H), 7.34–7.28 (m, 1H), 7.00 (t, *J* = 8.4 Hz, 2H), 4.69 (s, 1H), 2.97–2.13 (m, 4H), 1.86–1.41
16 (m, 6H); MS (ESI) *m/z* = 338.1 [M + H]⁺. Purity 100.0%.
17
18
19
20
21
22
23
24
25

26 **5-((4-Fluorophenyl)(piperidin-1-yl)methyl)benzo[*d*]thiazol-4-ol (5f)**. Prepared from 4-
27 fluorobenzaldehyde (50 mg, 0.40 mmol), benzo[*d*]thiazol-4-ol (50 mg, 0.33 mmol), and piperidine
28 (34 mg, 0.40 mmol) in toluene at 100 °C overnight. After concentration, the residue was purified
29 by silica column chromatography (hexane : EtOAc = 1:1) to give compound **5f** as a white solid
30 (46% yield). ¹H NMR (300 MHz, CDCl₃) δ 8.89 (s, 1H), 7.43 (t, *J* = 6.9 Hz, 2H), 7.27 (d, *J* = 8.3
31 Hz, 1H), 6.99 (q, *J* = 8.7 Hz, 3H), 4.63 (s, 1H), 2.80–2.32 (m, 4H), 1.79–1.40 (m, 6H); MS (ESI)
32 *m/z* = 343.5 [M + H]⁺. Purity 96.3%.
33
34
35
36
37
38
39
40
41

42 **6-((4-Fluorophenyl)(piperidin-1-yl)methyl)benzofuran-7-ol (5g)**. Prepared from 4-
43 fluorobenzaldehyde (32 mg, 0.26 mmol), benzofuran-7-ol (35 mg, 0.26 mmol), and piperidine (27
44 mg, 0.31 mmol) in toluene at 100 °C overnight. After concentration, the residue was purified by
45 silica column chromatography (hexane : EtOAc = 10:1) to give compound **5g** as a white solid (12
46 mg, 14% yield). ¹H NMR (300 MHz, CDCl₃) δ 7.63 (s, 1H), 7.42 (s, 2H), 7.07–6.91 (m, 3H), 6.76
47
48
49
50
51
52
53
54
55
56
57
58
59
60

(d, $J = 8.2$ Hz, 1H), 6.69 (s, 1H), 4.62 (s, 1H), 3.01–2.24 (m, 4H), 1.83–1.40 (m, 7H); MS (ESI) $m/z = 326.1$ [M + H]⁺. Purity 95.6%.

6-((4-Fluorophenyl)(piperidin-1-yl)methyl)-2,3-dihydrobenzo[*b*][1,4]dioxin-5-ol (5h).

Prepared from 4-fluorobenzaldehyde (62 mg, 0.50 mmol), 2,3-dihydrobenzo[*b*][1,4]dioxin-5-ol (50 mg, 0.33 mmol), and piperidine (43 mg, 0.50 mmol) in toluene at 100 °C overnight. After concentration, the residue was purified by silica column chromatography (hexane : EtOAc = 5:1) to give compound **5h** as a white solid (84 mg, 74% yield). ¹H NMR (300 MHz, CDCl₃) δ 7.44–7.30 (m, 2H), 6.99 (t, $J = 8.5$ Hz, 2H), 6.39–6.22 (m, 2H), 4.44 (s, 1H), 4.29 (ddd, $J = 26.8, 6.1, 3.3$ Hz, 4H), 2.98–2.18 (m, 4H), 1.77–1.36 (m, 6H); MS (ESI) $m/z = 344.4$ [M + H]⁺. Purity 99.4%.

5-((4-Fluorophenyl)(piperidin-1-yl)methyl)benzo[*d*][1,3]dioxol-4-ol (5i).

Prepared from 4-fluorobenzaldehyde (67 mg, 0.54 mmol), benzo[*d*][1,3]dioxol-4-ol (50 mg, 0.36 mmol), and piperidine (47 mg, 0.54 mmol) in toluene at 100 °C overnight. After concentration, the residue was purified by silica column chromatography (hexane : EtOAc = 1:1) to give compound **5i** as a white solid (82 mg, 69% yield). ¹H NMR (300 MHz, CDCl₃) δ 7.38 (t, $J = 6.6$ Hz, 2H), 7.01 (t, $J = 8.7$ Hz, 2H), 6.41–6.21 (m, 2H), 5.97 (dd, $J = 9.9, 1.4$ Hz, 2H), 4.49 (s, 1H), 2.93–2.18 (m, 4H), 1.75–1.38 (m, 6H); MS (ESI) $m/z = 330.5$ [M + H]⁺. Purity 97.8%.

6-((4-Fluorophenyl)(piperidin-1-yl)methyl)isoquinolin-5-ol (5j).

Prepared from 4-fluorobenzaldehyde (64 mg, 0.52 mmol), 5-hydroxyisoquinoline (50 mg, 0.34 mmol), and piperidine (44 mg, 0.52 mmol) in EtOH under microwave at 120 °C for 45 min. After concentration, the residue was purified by silica column chromatography (hexane : EtOAc = 5:1) to give compound **5j** as a white solid (37 mg, 32% yield). ¹H NMR (300 MHz, CDCl₃) δ 9.12 (s, 1H), 8.52 (d, $J = 5.9$ Hz, 1H), 8.08 (d, $J = 5.8$ Hz, 1H), 7.39 (t, $J = 7.1$ Hz, 2H), 7.33 (d, $J = 8.4$

1
2
3 Hz, 1H), 7.10 (d, $J = 8.4$ Hz, 1H), 7.01 (t, $J = 8.7$ Hz, 2H), 4.60 (s, 1H), 3.15–2.11 (m, 4H), 1.86–
4
5 1.40 (m, 6H); MS (ESI) $m/z = 337.1$ [M + H]⁺. Purity 95.7%.

6
7
8 **5-((4-Fluorophenyl)(piperidin-1-yl)methyl)-2,3-dihydro-1H-inden-4-ol (5k)**. Prepared from 4-
9
10 fluorobenzaldehyde (74 mg, 0.60 mmol), 2,3-dihydro-1H-inden-4-ol (80 mg, 0.60 mmol), and
11
12 piperidine (74 mg, 0.60 mmol) in toluene at 100 °C overnight. After concentration, the residue was
13
14 purified by silica column chromatography (hexane : EtOAc = 5:1) to give compound **5k** as a white
15
16 solid (49 mg, 17% yield). ¹H NMR (300 MHz, CDCl₃): δ 12.49 (s, 1H), 7.40 (t, $J = 6.7$ Hz, 2H),
17
18 7.01 (t, $J = 8.8$ Hz, 2H), 6.74–6.59 (m, 2H), 4.48 (s, 1H), 2.91 (dt, $J = 19.3, 7.4$ Hz, 4H), 2.42 (s,
19
20 4H), 2.11 (p, $J = 7.4$ Hz, 2H), 1.75–1.39 (m, 6H); MS (ESI) $m/z = 326.6$ [M + H]⁺. Purity 100.0%.

21
22
23 **2-(Dimethylamino)-6-((4-fluorophenyl)(piperidin-1-yl)methyl)phenol (5l)**. Prepared from 4-
24
25 fluorobenzaldehyde (68 mg, 0.55 mmol), 2-(dimethylamino)phenol (50 mg, 0.36 mmol), and
26
27 piperidine (47 mg, 0.55 mmol) in toluene at 100 °C overnight. After concentration, the residue
28
29 was purified by silica column chromatography (hexane : EtOAc = 5:1) to give compound **5l** as a
30
31 white solid (20 mg, 17% yield). ¹H NMR (300 MHz, CDCl₃) δ 12.73 (s, 1H), 7.42 (t, $J = 6.7$ Hz,
32
33 2H), 6.99 (t, $J = 8.5$ Hz, 2H), 6.84 (d, $J = 7.8$ Hz, 1H), 6.68 (t, $J = 7.7$ Hz, 1H), 6.60 (s, 1H), 4.44
34
35 (s, 1H), 2.84 (s, 6H), 2.73–2.19 (m, 4H), 1.80–1.35 (m, 6H). MS (ESI) $m/z = 329.0$ [M + H]⁺.
36
37 Purity 100.0%.

38
39
40
41
42
43 **1-(6-((4-Fluorophenyl)(piperidin-1-yl)methyl)-7-hydroxybenzofuran-2-yl)ethanone (5m)**.
44
45 Prepared from 4-fluorobenzaldehyde (112 mg, 0.90 mmol), 1-(7-hydroxybenzofuran-2-
46
47 yl)ethanone (160 mg, 0.90 mmol), and piperidine (92 mg, 1.10 mmol) in toluene at 100 °C
48
49 overnight. After concentration, the residue was purified by silica column chromatography (hexane
50
51 : EtOAc = 5:1) to give compound **5m** as a white solid (110 mg, 33% yield). ¹H NMR (400 MHz,
52
53

1
2
3 CDCl₃) δ 7.43 (s, 3H), 7.08–6.95 (m, 3H), 6.84 (s, 1H), 4.64 (s, 1H), 2.68 (s, 3H), 2.63–2.27 (m,
4 4H), 1.82–1.37 (m, 6H); MS (ESI) m/z = 368.3 [M + H]⁺. Purity 96.1%.

7
8 **6-((4-Fluoro-2-hydroxyphenyl)(piperidin-1-yl)methyl)benzofuran-7-ol (5n)**. Prepared from 4-
9 fluoro-2-hydroxybenzaldehyde (57 mg, 0.41 mmol), benzofuran-7-ol (50 mg, 0.37 mmol), and
10 piperidine in toluene at 100 °C overnight. After concentration, the residue was purified by silica
11 column chromatography (hexane : EtOAc = 5:1) to give compound **5n** as a white solid (26 mg,
12 21% yield). ¹H NMR (300 MHz, CDCl₃) δ 7.62 (d, J = 2.0 Hz, 1H), 7.03 (d, J = 7.8 Hz, 3H), 6.73
13 (d, J = 2.0 Hz, 1H), 6.62 (dd, J = 10.5, 2.5 Hz, 1H), 6.44 (dd, J = 9.6, 7.3 Hz, 1H), 5.22 (s, 1H),
14 3.05–2.35 (s, 4H), 1.79–1.41 (m, 6H); MS (ESI) m/z = 342.2 [M + H]⁺. Purity 95.6%.

15
16
17
18
19
20
21
22
23
24
25 **6-((2,3-Dihydro-1H-inden-5-yl)(piperidin-1-yl)methyl)benzofuran-7-ol (5o)**. Prepared from
26 2,3-dihydro-1H-indene-5-carbaldehyde (82 mg, 0.56 mmol), benzofuran-7-ol (50 mg, 0.37 mmol),
27 and piperidine (47 mg, 0.56 mmol) in toluene at 100 °C overnight. After concentration, the residue
28 was purified by silica column chromatography (hexane : EtOAc = 5:1) to give compound **5o** as a
29 white solid (52 mg, 41% yield). ¹H NMR (300 MHz, CDCl₃) δ 7.61 (d, J = 1.9 Hz, 1H), 7.35 (s,
30 1H), 7.24 (d, J = 8.0 Hz, 1H), 7.16 (d, J = 7.6 Hz, 1H), 6.99–6.82 (m, 2H), 6.68 (d, J = 2.0 Hz,
31 1H), 4.69 (s, 1H), 3.04–2.24 (m, 8H), 2.13–1.98 (m, 2H), 1.86–1.36 (m, 6H); MS (ESI) m/z =
32 348.2 [M + H]⁺. Purity 96.8%.

33
34
35
36
37
38
39
40
41
42
43 **6-(Piperidin-1-yl(pyridin-4-yl)methyl)benzofuran-7-ol (5p)**. Prepared from isonicotinaldehyde
44 (36 mg, 0.34 mmol), benzofuran-7-ol (30 mg, 0.22 mmol), and piperidine (29 mg, 0.34 mmol) in
45 toluene at 100 °C overnight. After concentration, the residue was purified by silica column
46 chromatography (hexane : EtOAc = 1:1) to give compound **5p** as a white solid (36 mg, 53% yield).
47
48
49
50
51
52
53 ¹H NMR (300 MHz, CDCl₃) δ 8.55 (d, J = 5.2 Hz, 2H), 7.63 (d, J = 2.0 Hz, 1H), 7.41 (d, J = 5.0

1
2
3 Hz, 2H), 6.96 (d, $J = 8.0$ Hz, 1H), 6.77 (d, $J = 8.0$ Hz, 1H), 6.69 (d, $J = 2.0$ Hz, 1H), 4.55 (s, 1H),
4
5 2.91–2.36 (m, 4H), 1.81–1.43 (m, 7H); MS (ESI) $m/z = 309.2$ [M + H]⁺. Purity 99.8%.

6
7
8 **6-((2,2-Difluorobenzo[*d*][1,3]dioxol-5-yl)(piperidin-1-yl)methyl)benzofuran-7-ol (5q).**

9
10 Prepared from 2,2-difluorobenzo[*d*][1,3]dioxole-5-carbaldehyde (49 mg, 0.26 mmol), benzofuran-
11
12 7-ol (30 mg, 0.22 mmol), and piperidine (29 mg, 0.34 mmol) in toluene at 100 °C overnight. After
13
14 concentration, the residue was purified by silica column chromatography (hexane : DCM = 9:1) to
15
16 give compound **5q** as a white solid (16 mg, 19% yield). ¹H NMR (300 MHz, CDCl₃) δ 7.64 (d, J
17
18 = 2.2 Hz, 1H), 7.27 (d, $J = 4.5$ Hz, 1H), 7.14 (d, $J = 8.4$ Hz, 1H), 7.03–6.91 (m, 2H), 6.76 (d, $J =$
19
20 7.9 Hz, 1H), 6.70 (d, $J = 2.1$ Hz, 1H), 4.58 (s, 1H), 2.95–2.22 (s, 4H), 1.81–1.43 (m, 6H); MS
21
22 (ESI) $m/z = 388.2$ [M + H]⁺. Purity 99.6%.

23
24
25
26 **6-(Piperidin-1-yl(4-(trifluoromethyl)phenyl)methyl)benzofuran-7-ol (5r).** Prepared from 4-

27
28 (trifluoromethyl)benzaldehyde (59 mg, 0.34 mmol), benzofuran-7-ol (30 mg, 0.22 mmol), and
29
30 piperidine (29 mg, 0.34 mmol) in toluene at 100 °C overnight. After concentration, the residue
31
32 was purified by silica column chromatography (hexane : EtOAc = 5:1) to give compound **5r** as a
33
34 white solid (28 mg, 34% yield). ¹H NMR (400 MHz, CDCl₃) δ 7.67–7.49 (m, 5H), 6.93 (d, $J = 8.0$
35
36 Hz, 1H), 6.74 (d, $J = 8.0$ Hz, 1H), 6.67 (d, $J = 2.1$ Hz, 1H), 4.63 (s, 1H), 3.08–2.18 (m, 4H), 1.78–
37
38 1.39 (m, 6H); MS (ESI) $m/z = 376.1$ [M + H]⁺. Purity 99.8%.

39
40
41
42 **6-((2,3-Dimethoxyphenyl)(morpholino)methyl)benzo[*d*][1,3]dioxol-5-ol (6a).** Prepared from

43
44 2,3-dimethoxybenzaldehyde (5.00 g, 30.1 mmol), benzo[*d*][1,3]dioxol-5-ol (4.16 g, 30.1 mmol),
45
46 and morpholine (2.62 g, 30.1 mmol) in EtOH reflux overnight, and recrystallized from
47
48 MeOH/acetone to give compound **6a** as a white solid (6.40 g, 57% yield). ¹H NMR (300 MHz,
49
50 CDCl₃): δ 11.75 (s, 1H), 7.13 (d, $J = 8.0$ Hz, 1H), 7.00 (t, $J = 8.0$ Hz, 1H), 6.81 (d, $J = 8.1$ Hz,
51
52
53
54
55
56
57
58
59
60

1
2
3 1H), 6.42 (d, $J = 11.5$ Hz, 2H), 5.81 (dd, $J = 13.0, 1.3$ Hz, 2H), 4.98 (s, 1H), 3.99–3.83 (m, 6H),
4
5 3.79–3.64 (m, 4H), 2.83–2.36 (m, 4H); MS (ESI) $m/z = 374.0$ [M + H]⁺. Purity 95.5%.

6
7 **6-(phenyl(piperidin-1-yl)methyl)benzo[*d*][1,3]dioxol-5-ol (6b)**. Prepared from benzaldehyde
8
9 (115 mg, 1.09 mmol), benzo[*d*][1,3]dioxol-5-ol (100 mg, 0.72 mmol), and piperidine (93 mg, 1.09
10
11 mmol) in toluene at 100 °C overnight. After concentration, the residue was purified by silica
12
13 column chromatography (hexane : EtOAc = 5:1) to give compound **6b** as a white solid (120 mg,
14
15 54% yield). ¹H NMR (300 MHz, DMSO-*d*₆) δ 11.12 (s, 1H), 7.39 (d, $J = 7.6$ Hz, 2H), 7.30 (t, $J =$
16
17 7.5 Hz, 2H), 7.27–7.15 (m, 1H), 6.65 (s, 1H), 6.36 (s, 1H), 5.84 (d, $J = 3.3$ Hz, 2H), 4.50 (s, 1H),
18
19 2.47–2.21 (m, 4H), 1.60–1.33 (m, 6H). MS (ESI) $m/z = 312.0$ [M + H]⁺. Purity 99.6%.

20
21 **7-((4-Fluorophenyl)(piperidin-1-yl)methyl)-2,3-dihydrobenzo[*b*][1,4]dioxin-6-ol (6c)**.
22
23 Prepared from 4-fluorobenzaldehyde (45 mg, 0.36 mmol), 2,3-dihydrobenzo[*b*][1,4]dioxin-6-ol
24
25 (50 mg, 0.33 mmol), and piperidine (31 mg, 0.36 mmol) in toluene at 100 °C overnight. After
26
27 concentration, the residue was purified by silica column chromatography (hexane : EtOAc = 5:1)
28
29 to give compound **6c** as a white solid (40 mg, 35% yield). ¹H NMR (300 MHz, CDCl₃) δ 12.04 (s,
30
31 1H), 7.37 (t, $J = 6.8$ Hz, 2H), 7.01 (t, $J = 8.5$ Hz, 2H), 6.41 (s, 2H), 4.40 (s, 1H), 4.26–4.10 (m,
32
33 4H), 2.80–2.21 (m, 4H), 1.78–1.39 (m, 6H); MS (ESI) $m/z = 344.2$ [M + H]⁺. Purity 100.0%.

34
35 **6-((4-Fluorophenyl)(piperidin-1-yl)methyl)indolin-5-ol (6d)**. Starting from 4-
36
37 fluorobenzaldehyde (29 mg, 0.23 mmol), *tert*-butyl 5-hydroxyindoline-1-carboxylate (50 mg, 0.21
38
39 mmol), and piperidine (20 mg, 0.23 mmol) in toluene at 100 °C overnight. After concentration,
40
41 the residue was purified by silica column chromatography (hexane : EtOAc = 1:1) to give *tert*-
42
43 butyl 6-((4-fluorophenyl)(piperidin-1-yl)methyl)-5-hydroxyindoline-1-carboxylate (34 mg, 38%
44
45 yield), which was directly dissolved in DCM (3 mL), and a solution of HCl in dioxane (4N, 0.6
46
47 mL) was added. The mixture was stirred at room temperature for 3h, concentrated and purified by
48
49
50
51
52
53
54
55
56
57
58
59
60

1
2
3 silica column chromatography (DCM : MeOH = 30:1) to give **6d** as a white solid (12 mg, 46%
4 yield). ¹H NMR (300 MHz, MeOD) δ 7.97 (s, 1H), 7.87 (t, J = 6.6 Hz, 2H), 7.20 (t, J = 8.3 Hz,
5 2H), 7.06 (s, 1H), 5.83 (s, 1H), 3.92–3.46 (m, 5H), 3.26–3.32 (m, 1H), 3.18–2.99 (m, 2H), 2.10–
6 1.79 (m, 5H), 1.68–1.53 (m, 1H); MS (ESI) m/z = 327.1 [M + H]⁺. Purity 96.6%.
7
8
9
10
11
12

13 **6-((2,3-Dimethoxyphenyl)(morpholino)methyl)-2,2-difluorobenzo[*d*][1,3]dioxol-5-ol (6e).**

14 Prepared from 2,3-dimethoxybenzaldehyde (52 mg, 0.32 mmol), 2,2-difluorobenzo[*d*][1,3]dioxol-
15 5-ol (55 mg, 0.32 mmol), and morpholine (27 mg, 0.32 mmol) in toluene at 100 °C overnight.
16 After concentration, the residue was purified by silica column chromatography (hexane : EtOAc
17 = 1:1) to give compound **6e** as a white solid (18 mg, 14% yield). ¹H NMR (300 MHz, CDCl₃): δ
18 12.23 (s, 1H), 7.15–7.08 (m, 1H), 7.04 (t, J = 7.9 Hz, 1H), 6.86 (dd, J = 7.9, 1.7 Hz, 1H), 6.70 (s,
19 1H), 6.60 (s, 1H), 5.10 (s, 1H), 3.93 (s, 3H), 3.90 (s, 3H), 3.82–3.73 (m, 4H), 2.91–2.45 (m, 6H);
20 MS (ESI) m/z = 410.5 [M + H]⁺. Purity 95.9%.
21
22
23
24
25
26
27
28
29
30

31 **6-((4-Fluorophenyl)(piperidin-1-yl)methyl)-2,3-dihydro-1*H*-inden-5-ol (6f).** Prepared from 4-

32 fluorobenzaldehyde (89 mg, 0.72 mmol), 2,3-dihydro-1*H*-inden-5-ol (80 mg, 0.60 mmol), and
33 piperidine (61 mg, 0.72 mmol) in toluene at 100 °C overnight. After concentration, the residue
34 was purified by silica column chromatography (hexane : EtOAc = 10:1) to give compound **6f** as a
35 white solid (94 mg, 48% yield). ¹H NMR (300 MHz, CDCl₃) δ 12.23 (s, 1H), 7.42 (t, J = 6.6 Hz,
36 2H), 7.01 (t, J = 8.5 Hz, 2H), 6.76 (d, J = 8.2 Hz, 2H), 4.41 (s, 1H), 2.84 (t, J = 7.5 Hz, 2H), 2.74
37 (t, J = 7.7 Hz, 2H), 2.40 (s, 4H), 2.10–1.96 (m, 2H), 1.76–1.40 (m, 6H); MS (ESI) m/z = 326.1 [M
38 + H]⁺. Purity 98.3%.
39
40
41
42
43
44
45
46
47
48
49

50 **3-((4-Fluorophenyl)(piperidin-1-yl)methyl)-5,6,7,8-tetrahydronaphthalen-2-ol (6g).** Prepared

51 from 4-fluorobenzaldehyde (63 mg, 0.51 mmol), 5,6,7,8-tetrahydronaphthalen-2-ol (50 mg, 0.34
52 mmol), and piperidine (44 mg, 0.51 mmol) in EtOH under microwave at 120 °C for 45 min. After
53
54
55
56
57
58
59
60

1
2
3 concentration, the residue was purified by silica column chromatography (hexane : EtOAc = 5:1)
4
5 to give compound **6g** as a white solid (10 mg, 9% yield). ¹H NMR (300 MHz, CDCl₃) δ 7.40 (s,
6
7 2H), 7.01 (t, *J* = 8.5 Hz, 2H), 6.59 (s, 2H), 4.39 (s, 1H), 2.80–2.26 (m, 8H), 1.78–1.42 (m, 10H);
8
9 MS (ESI) *m/z* = 340.2 [M + H]⁺. Purity 96.4%.

10
11
12 **5-((4-Fluorophenyl)(piperidin-1-yl)methyl)quinolin-6-ol (7a)**. Prepared from 4-
13
14 fluorobenzaldehyde (53 mg, 0.62 mmol), 6-hydroxyquinoline (60 mg, 0.41 mmol), and piperidine
15
16 (77 mg, 0.62 mmol) in toluene at 100 °C overnight. After concentration, the residue was purified
17
18 by silica column chromatography (hexane : EtOAc = 5:1) to give compound **7a** as a white solid
19
20 (30 mg, 22% yield). ¹H NMR (300 MHz, CDCl₃) δ 13.99 (s, 1H), 8.64 (dd, *J* = 4.1, 1.4 Hz, 1H),
21
22 8.11 (d, *J* = 8.6 Hz, 1H), 7.94 (d, *J* = 9.1 Hz, 1H), 7.54–7.43 (m, 2H), 7.38 (d, *J* = 9.1 Hz, 1H),
23
24 7.24 (dd, *J* = 8.7, 4.2 Hz, 1H), 6.95 (t, *J* = 8.5 Hz, 2H), 5.00 (s, 1H), 3.33–1.48 (s, 10H); MS (ESI)
25
26 *m/z* = 337.2 [M + H]⁺. Purity 97.4%.

27
28
29
30
31 **4-((4-Fluorophenyl)(piperidin-1-yl)methyl)benzo[d]thiazol-5-ol (7b)**. Prepared from 4-
32
33 fluorobenzaldehyde (50 mg, 0.40 mmol), 5-hydroxybenzothiazole (50 mg, 0.33 mmol), and
34
35 piperidine (34 mg, 0.40 mmol) in EtOH under microwave at 120 °C for 45 min. After
36
37 concentration, the residue was purified by silica column chromatography (hexane : EtOAc = 5:1)
38
39 to give compound **7b** as a white solid (60 mg, 53% yield). ¹H NMR (300 MHz, CDCl₃) δ 12.77 (s,
40
41 1H), 8.68 (s, 1H), 7.88 (d, *J* = 8.8 Hz, 1H), 7.49 (t, *J* = 6.8 Hz, 2H), 7.11 (d, *J* = 8.8 Hz, 1H), 6.99
42
43 (t, *J* = 8.6 Hz, 2H), 4.45 (s, 1H), 2.78–2.19 (s, 4H), 1.80–1.32 (m, 6H); MS (ESI) *m/z* = 343.1 [M
44
45 + H]⁺. Purity 96.4%.

46
47
48
49 **5-((4-Fluorophenyl)(piperidin-1-yl)methyl)quinoxalin-6-ol (7c)**. Prepared from 4-
50
51 fluorobenzaldehyde (64 mg, 0.52 mmol), quinoxaline-6-ol (50 mg, 0.34 mmol), and piperidine (44
52
53 mg, 0.52 mmol) in EtOH under microwave at 120 °C for 45 min. After concentration, the residue
54
55

1
2
3 was purified by silica column chromatography (hexane : EtOAc = 5:1) to give compound **7c** as a
4 white solid (32 mg, 28% yield). ¹H NMR (300 MHz, CDCl₃) δ 8.66 (d, *J* = 1.9 Hz, 1H), 8.59 (d, *J*
5 = 1.9 Hz, 1H), 7.90 (d, *J* = 9.1 Hz, 1H), 7.61 (dd, *J* = 8.5, 5.5 Hz, 2H), 7.48 (d, *J* = 9.2 Hz, 1H),
6 6.94 (t, *J* = 8.6 Hz, 2H), 5.84 (s, 1H), 3.61–1.21 (m, 10H); MS (ESI) *m/z* = 338.4 [M + H]⁺. Purity
7 98.6%.
8
9

10
11
12
13
14
15 **8-((4-Fluorophenyl)(piperidin-1-yl)methyl)isoquinolin-7-ol (7d)**. Prepared from 4-
16 fluorobenzaldehyde (89 mg, 0.72 mmol), isoquinolin-7-ol (80 mg, 0.48 mmol), and piperidine in
17 toluene at 100 °C overnight. After concentration, the residue was purified by silica column
18 chromatography (hexane : EtOAc = 3:1) to give compound **7d** as a white solid (94 mg, 58% yield).
19
20
21
22
23
24 ¹H NMR (300 MHz, CDCl₃) δ 14.24 (s, 1H), 9.31 (s, 1H), 8.33 (d, *J* = 5.4 Hz, 1H), 7.67 (d, *J* =
25 8.8 Hz, 1H), 7.53 (t, *J* = 8.0 Hz, 3H), 7.38 (d, *J* = 8.8 Hz, 1H), 6.98 (t, *J* = 8.1 Hz, 2H), 5.24 (s,
26 1H), 3.30 (s, 1H), 2.76–1.52 (m, 9H); MS (ESI) *m/z* = 337.1 [M + H]⁺. Purity 97.4%.
27
28
29
30

31
32
33
34
35
36
37
38
39
40
41
42
43
44
45
46
47
48
49
50
51
52
53
54
55
56
57
58
59
60
5-((4-Fluorophenyl)(piperidin-1-yl)methyl)isoquinolin-6-ol (7e). Prepared from 4-
fluorobenzaldehyde (89 mg, 0.72 mmol), isoquinolin-6-ol (80 mg, 0.48 mmol), and piperidine (62
mg, 0.72 mmol) in toluene at 100 °C overnight. After concentration, the residue was purified by
silica column chromatography (hexane : EtOAc = 3:1) to give compound **7e** as a white solid (103
mg, 64% yield). ¹H NMR (300 MHz, CDCl₃) δ 14.59 (s, 1H), 9.00 (s, 1H), 8.33 (d, *J* = 6.1 Hz,
1H), 7.80 (d, *J* = 8.9 Hz, 1H), 7.58–7.43 (m, 3H), 7.24 (d, *J* = 9.0 Hz, 1H), 6.99 (t, *J* = 8.5 Hz, 2H),
5.02 (s, 1H), 3.28 (s, 1H), 2.88–1.32 (m, 9H); MS (ESI) *m/z* = 337.1 [M + H]⁺. Purity 100.0%.

4-((4-Fluorophenyl)(piperidin-1-yl)methyl)-1*H*-indol-5-ol (7f). Prepared from 4-
fluorobenzaldehyde (112 mg, 0.90 mmol), 1*H*-indol-5-ol (80 mg, 0.60 mmol), and piperidine (77
mg, 0.90 mmol) under microwave at 120 °C for 45 min. After concentration, the residue was
purified by silica column chromatography (hexane : EtOAc = 5:1) to give compound **7f** as a white

1
2
3 solid (26 mg, 13% yield). ¹H NMR (300 MHz, CDCl₃) δ 8.07 (s, 1H), 7.55 (s, 2H), 7.18 (d, *J* =
4 8.5 Hz, 1H), 7.11 (d, *J* = 2.8 Hz, 1H), 7.01–6.84 (m, 3H), 6.38 (s, 1H), 4.81–4.71 (m, 1H), 3.12–
5 2.11 (m, 4H), 1.78–1.46 (m, 6H); MS (ESI) *m/z* = 325.1 [M + H]⁺. Purity 96.5%.
6
7

8
9
10 **4-((4-Fluorophenyl)(piperidin-1-yl)methyl)-1*H*-indazol-5-ol (7g)**. Prepared from 4-
11 fluorobenzaldehyde (69 mg, 0.56 mmol), 1*H*-indazol-5-ol (50 mg, 0.37 mmol), and piperidine (48
12 mg, 0.56 mmol) in EtOH under microwave at 120 °C for 45 min. After concentration, the residue
13 was purified by silica column chromatography (hexane : EtOAc = 3:1) to give compound **7g** as a
14 white solid (32 mg, 27% yield). ¹H NMR (300 MHz, CDCl₃) δ 12.24 (s, 1H), 7.85 (s, 1H), 7.49 (t,
15 *J* = 6.7 Hz, 2H), 7.26 (d, *J* = 10.0 Hz, 1H), 6.99 (dt, *J* = 17.0, 8.7 Hz, 3H), 4.74 (s, 1H), 2.94–2.20
16 (m, 4H), 1.83–1.37 (m, 6H); MS (ESI) *m/z* = 326.2 [M + H]⁺. Purity 95.2%.
17
18
19

20
21
22 **4-(Piperidin-1-yl(4-(trifluoromethyl)phenyl)methyl)-1*H*-indazol-5-ol (7h)**. Prepared from 4-
23 (trifluoromethyl)benzaldehyde (97 mg, 0.56 mmol), 1*H*-indazol-5-ol (50 mg, 0.37 mmol), and
24 piperidine (48 mg, 0.56 mmol) under microwave at 120 °C for 45 min. After concentration, the
25 residue was purified by silica column chromatography (hexane : EtOAc = 3:1) to give compound
26 **7h** as a white solid (90 mg, 65% yield). ¹H NMR (300 MHz, CDCl₃) δ 7.88 (s, 1H), 7.68 (d, *J* =
27 7.7 Hz, 2H), 7.55 (d, *J* = 8.0 Hz, 2H), 7.32–7.23 (m, 1H), 7.11–6.99 (m, 1H), 4.81 (s, 1H), 2.78–
28 2.11 (m, 4H), 1.83–1.41 (m, 6H). ; MS (ESI) *m/z* = 376.1 [M + H]⁺. Purity 99.6%.
29
30
31

32
33
34 **4-((4-Nitrophenyl)(piperidin-1-yl)methyl)-1*H*-indazol-5-ol (7i)**. Prepared from 4-
35 nitrobenzaldehyde (85 mg, 0.56 mmol), 1*H*-indazol-5-ol (50 mg, 0.37 mmol), and piperidine (48
36 mg, 0.56 mmol) under microwave at 120 °C for 45 min. After concentration, the residue was
37 purified by silica column chromatography (hexane : EtOAc = 3:1) to give compound **7i** as a white
38 solid (87 mg, 67% yield). ¹H NMR (300 MHz, CDCl₃) δ 8.20–8.11 (m, 2H), 7.89 (s, 1H), 7.74 (d,
39
40
41
42
43
44
45
46
47
48
49
50
51
52
53
54
55
56
57
58
59
60

$J = 8.2$ Hz, 2H), 7.31 (s, 2H), 7.05 (d, $J = 9.1$ Hz, 1H), 4.85 (s, 1H), 2.87–2.25 (m, 4H), 1.82–1.33 (m, 6H); MS (ESI) $m/z = 353.2$ [M + H]⁺. Purity 96.5%.

4-(Piperidin-1-yl(4-(thiazol-2-yl)phenyl)methyl)-1H-indazol-5-ol (7j). Prepared from 4-(thiazol-2-yl)benzaldehyde (84 mg, 0.44 mmol), 1H-indazol-5-ol (50 mg, 0.37 mmol), and piperidine (48 mg, 0.56 mmol) in toluene at 100 °C overnight. After concentration, the residue was purified by silica column chromatography (hexane : EtOAc = 5:1) to give compound **7j** as a white solid (102 mg, 70% yield). ¹H NMR (300 MHz, CDCl₃) δ 7.93–7.79 (m, 4H), 7.60 (d, $J = 8.0$ Hz, 2H), 7.27 (d, $J = 3.5$ Hz, 1H), 7.23 (d, $J = 8.8$ Hz, 1H), 7.01 (d, $J = 8.8$ Hz, 1H), 4.79 (s, 1H), 3.12–2.08 (m, 4H), 1.83–1.39 (m, 6H); MS (ESI) $m/z = 391.5$ [M + H]⁺. Purity 95.2%.

4-((4-(1H-Pyrrol-1-yl)phenyl)(piperidin-1-yl)methyl)-1H-indazol-5-ol (7k). Prepared from 4-(1H-pyrrol-1-yl)benzaldehyde (96 mg, 0.56 mmol), 1H-indazol-5-ol (50 mg, 0.37 mmol), and piperidine (48 mg, 0.56 mmol) in toluene at 100 °C overnight. After concentration, the residue was purified by silica column chromatography (hexane : EtOAc = 5:1) to give compound **7k** as a white solid (86 mg, 62% yield). ¹H NMR (300 MHz, CDCl₃) δ 7.90 (s, 1H), 7.58 (d, $J = 7.9$ Hz, 2H), 7.29 (t, $J = 8.3$ Hz, 3H), 7.10–6.99 (m, 3H), 6.32 (d, $J = 2.3$ Hz, 2H), 4.79 (s, 1H), 3.33–2.16 (m, 4H), 1.88–1.42 (m, 6H); MS (ESI) $m/z = 373.1$ [M + H]⁺. Purity 98.9%.

4-(Piperidin-1-yl(4-(pyrimidin-5-yl)phenyl)methyl)-1H-indazol-5-ol (7l). Prepared from 4-(pyrimidin-5-yl)benzaldehyde (103 mg, 0.56 mmol), 1H-indazol-5-ol (50 mg, 0.37 mmol), and piperidine (48 mg, 0.56 mmol) in toluene at 100 °C overnight. After concentration, the residue was purified by silica column chromatography (hexane : EtOAc = 5:1) to give compound **7l** as a white solid (52 mg, 37% yield). ¹H NMR (300 MHz, CDCl₃) δ 9.19 (d, $J = 1.6$ Hz, 1H), 8.89 (d, $J = 1.6$ Hz, 2H), 7.92 (s, 1H), 7.70 (d, $J = 7.8$ Hz, 2H), 7.49 (d, $J = 7.9$ Hz, 2H), 7.27 (d, $J = 7.9$ Hz,

1
2
3 1H), 7.05 (dd, $J = 8.9, 1.6$ Hz, 1H), 4.82 (s, 1H), 3.12–2.23 (m, 4H), 1.84–1.39 (m, 6H); MS (ESI)
4
5 $m/z = 386.1$ [M + H]⁺. Purity 97.3%.

6
7
8 **6-((4-(Dimethylamino)phenyl)(pyrimidin-2-ylamino)methyl)benzo[*d*][1,3]dioxol-5-ol (14).**

9
10 Prepared from 4-(dimethylamino)benzaldehyde (149 mg, 1.00 mmol), benzo[*d*][1,3]dioxol-5-ol
11
12 (138 mg, 1.00 mmol), and 2-aminopyrimidine (95 mg, 1.00 mmol) in toluene at 100 °C overnight.

13
14 After concentration, the residue was purified by silica column chromatography (hexane : EtOAc
15
16 = 2:1) to give compound **14** as a white solid (73 mg, 20% yield). ¹H NMR (300 MHz, CDCl₃): δ
17
18 10.11 (s, 1H), 8.30 (d, $J = 4.9$ Hz, 2H), 7.25 (d, $J = 8.5$ Hz, 2H), 6.60 (t, $J = 4.9$ Hz, 1H), 6.50 (d,
19
20 $J = 4.3$ Hz, 2H), 6.44–6.31 (m, 2H), 5.89–5.79 (m, 2H), 2.96 (s, 6H); MS (ESI) $m/z = 365.2$ [M +
21
22 H]⁺. Purity 96.6%.

23
24
25
26 **1-((4-Fluorophenyl)(7-methoxybenzofuran-6-yl)methyl)piperidine (8). 5g** (32 mg, 0.098

27
28 mmol) was dissolved in acetone (3 mL), and K₂CO₃ (41 mg, 0.294 mmol) and Me₂SO₄ (19 mg,
29
30 0.148 mmol) were added. The mixture was stirred at room temperature for 6 h and concentrated.

31
32 The residue was purified by silica column chromatography (hexane : EtOAc = 5:1) to give **8** as a
33
34 white solid (10 mg, 30% yield). ¹H NMR (300 MHz, CDCl₃) δ 7.57 (d, $J = 2.2$ Hz, 1H), 7.51–7.40
35
36 (m, 3H), 7.24 (d, $J = 8.1$ Hz, 1H), 6.95 (t, $J = 8.7$ Hz, 2H), 6.71 (d, $J = 2.2$ Hz, 1H), 4.87 (s, 1H),
37
38 4.11 (s, 3H), 2.45–2.25 (m, 4H), 1.66–1.42 (m, 6H). MS (ESI) $m/z = 340.3$ [M + H]⁺. Purity 98.2%.

39
40
41
42 **(6-Hydroxybenzo[*d*][1,3]dioxol-5-yl)(phenyl)methanone (10).** MeI (1.29 g, 9.05 mmol) was

43
44 added to a suspension of Mg beads (130 mg, 5.43 mmol) in dry Et₂O (3 mL) at 35 °C under argon.

45
46
47 When the Mg beads were dissolved, a solution of benzo[*d*][1,3]dioxol-5-ol (**9**, 511 mg, 3.62 mmol)
48
49 in Et₂O (2 mL) was added, and the resulting solution was stirred at room temperature for 1 h. The
50
51 solvent was then evaporated, and toluene (3 mL) was added. Benzoyl chloride (511 mg, 3.62
52
53 mmol) in toluene was added dropwise at 0 °C. The mixture was stirred at room temperature for 12
54
55

h and quenched with sat. NH_4Cl . The product was extracted with EtOAc, and the organic layer was washed with brine and dried over anhydrous Na_2SO_4 . The crude product was purified with flash chromatography (10% EtOAc in hexane) to give **10** as a white solid (570 mg, 65%). ^1H NMR (300 MHz, CDCl_3) δ 13.03 (s, 1H), 7.67–7.47 (m, 5H), 6.97 (s, 1H), 6.57 (s, 1H), 6.01 (s, 2H).

6-(Cyclohexyl(hydroxy)(phenyl)methyl)benzo[*d*][1,3]dioxol-5-ol (11). To an ice-cooled solution of **10** in Et_2O was added cyclohexylmagnesium bromide (0.58 mL, 0.58 mmol, 1 M in THF) dropwise under argon. The mixture was heated at 50 °C for 3 h and cooled. Saturated NH_4Cl was added to quench the reaction, and the mixture was extracted by EtOAc. The organic layer was washed with brine and dried over anhydrous Na_2SO_4 . The crude product was purified with flash chromatography (20% EtOAc in hexane) to give **11** as a white solid (30 mg, 54%). ^1H NMR (300 MHz, MeOD) δ 7.42 (d, $J = 7.8$ Hz, 2H), 7.27 (t, $J = 7.6$ Hz, 2H), 7.16 (t, $J = 7.3$ Hz, 1H), 6.71 (s, 1H), 6.23 (d, $J = 1.0$ Hz, 1H), 5.83 (d, $J = 6.6$ Hz, 2H), 2.33 (t, $J = 10.3$ Hz, 1H), 1.91–1.65 (m, 4H), 1.43–1.10 (m, 6H). ^{13}C NMR (101 MHz, CDCl_3) δ 152.00, 147.24, 144.44, 140.46, 128.20, 126.95, 125.61, 119.53, 106.48, 101.00, 99.60, 84.04, 46.18, 27.47, 26.65, 26.59, 26.54, 26.42. MS (ESI) $m/z = 325.3$ [$\text{M} - \text{H}$] $^-$.

6-(Cyclohexylidene(phenyl)methyl)benzo[*d*][1,3]dioxol-5-ol (12). To a solution of **11** (12 mg, 0.037 mmol) in toluene was added TsOH (1 mg) and stirred at room temperature for 2 h. The mixture was concentrated and purified with flash chromatography (10% EtOAc in hexane) to give **12** as a light-yellow solid (11 mg, 96%). ^1H NMR (300 MHz, MeOD) δ 7.30–7.09 (m, 5H), 6.38 (s, 2H), 5.82 (d, $J = 5.5$ Hz, 2H), 2.40–2.27 (m, 1H), 2.27–2.08 (m, 3H), 1.78–1.44 (m, 6H). ^{13}C NMR (101 MHz, CDCl_3) δ 147.29, 147.12, 147.03, 143.89, 141.34, 141.13, 129.24, 128.22, 126.68, 120.30, 109.24, 100.95, 97.17, 32.64, 31.93, 28.79, 28.41, 26.55.

6-(Cyclohexyl(phenyl)methyl)benzo[*d*][1,3]dioxol-5-ol (13). To a solution of **8** (46 mg, 0.15 mmol) in EtOH (5 mL) was added Pd/C (9.2 mg). The mixture was heated at 60 °C under H₂ for 3 h, cooled, and filtered. The filtrate was concentrated and purified with flash chromatography (20% EtOAc in hexane) to give **13** as a white solid (36 mg, 77%). ¹H NMR (400 MHz, CDCl₃) δ 7.29 (d, *J* = 4.3 Hz, 4H), 7.18 (p, *J* = 4.4 Hz, 1H), 6.86 (s, 1H), 6.33 (s, 1H), 5.89 (dd, *J* = 16.8, 1.4 Hz, 2H), 4.59 (s, 1H), 3.87 (d, *J* = 10.8 Hz, 1H), 2.12–2.00 (m, 1H), 1.85–1.64 (m, 3H), 1.61–1.53 (m, 1H), 1.36–1.13 (m, 4H), 1.03–0.86 (m, 2H). MS (ESI) *m/z* = 311.0 [M – H][–]. Purity 97.3%.

Synthesis of BODIPY-labeled compounds

4-((6-Hydroxybenzo[*d*][1,3]dioxol-5-yl)(piperidin-1-yl)methyl)benzoic acid (S4). A mixture of benzo[*d*][1,3]dioxol-5-ol (1.00 g, 7.25 mmol), 4-formylbenzoic acid (1.09 g, 7.25 mmol), and piperidine (0.62 g, 7.25 mmol) were heated in toluene at 100 °C overnight. The precipitate generated was filtered, washed with toluene three times, and dried to give **S4** as a white solid (2.10 g, 82%). ¹H NMR (300 MHz, MeOD) δ 7.89 (d, *J* = 7.9 Hz, 2H), 7.42 (d, *J* = 7.9 Hz, 2H), 6.45 (d, *J* = 1.8 Hz, 1H), 6.34 (d, *J* = 1.9 Hz, 1H), 5.79 (d, *J* = 9.1 Hz, 2H), 4.49 (s, 1H), 2.73–2.31 (m, 4H), 1.68–1.39 (m, 6H). MS (ESI) *m/z* = 356.1 [M + H]⁺.

***N*-(4-(5,5-Difluoro-1,3,7,9-tetramethyl-5*H*-4λ⁴,5λ⁴-dipyrrolo[1,2-*c*:2',1'-**

***f*][1,3,2]diazaborinin-10-yl)phenyl)-4-((6-hydroxybenzo[*d*][1,3]dioxol-5-yl)(piperidin-1-**

yl)methyl)benzamide (15). To a solution of **S4** (30 mg, 0.085 mmol) in DMF (2 mL) was added EDCI (13 mg, 0.085 mmol) and HOBt (11 mg, 0.085 mmol) followed by 4-(5,5-difluoro-1,3,7,9-tetramethyl-5*H*-4λ⁴,5λ⁴-dipyrrolo[1,2-*c*:2',1'-*f*][1,3,2]diazaborinin-10-yl)aniline (BODIPY aniline, 29 mg, 0.085 mmol). The mixture was stirred at room temperature overnight and partitioned between EtOAc and water. The organic layer was washed with water twice, brine once and dried

over anhydrous Na₂SO₄. The mixture was then filtered and concentrated. The residue was purified with prep-HPLC (acetonitrile/water (10–95%)) over 25 min at an 8 mL/min flow rate at room temperature) to give **15** as a red solid (8.6 mg, 15%). ¹H NMR (300 MHz, DMSO) δ 9.51 (s, 1H), 7.40 (d, *J* = 7.9 Hz, 2H), 7.31 (d, *J* = 7.8 Hz, 2H), 6.95 (d, *J* = 8.1 Hz, 2H), 6.83–6.71 (m, 3H), 6.63 (d, *J* = 7.5 Hz, 1H), 6.46 (s, 1H), 6.13 (s, 2H), 5.89 (dd, *J* = 15.7, 6.4 Hz, 3H), 3.31–3.19 (m, 4H), 2.42 (s, 6H), 1.66–1.46 (m, 6H), 1.41 (s, 6H). MS (ESI) *m/z* = 675.5 [*M* - H]⁻. Purity 98.1%.

***tert*-Butyl (2-(4-((6-hydroxybenzo[*d*][1,3]dioxol-5-yl)(piperidin-1-yl)methyl)benzamido)ethyl)carbamate (S5).** To a solution of **S4** (200 mg, 0.56 mmol) and *tert*-butyl (2-aminoethyl)carbamate (108 mg, 0.68 mmol) in DMF (1 mL) was added HATU (319 mg, 0.84 mmol) and DIEA (217 mg, 1.68 mmol). The mixture was stirred at room temperature overnight and partitioned between EtOAc and water. The organic layer was washed with water twice, brine once, and dried over anhydrous Na₂SO₄. The mixture was then filtered and concentrated. The residue was purified with flash chromatography (30% EtOAc in hexane) to give **S5** as a light yellow solid (168 mg, 60%). ¹H NMR (300 MHz, DMSO-*d*₆) δ 10.82 (s, 1H), 8.38 (d, *J* = 5.5 Hz, 1H), 7.75 (d, *J* = 8.0 Hz, 2H), 7.45 (d, *J* = 8.1 Hz, 2H), 6.89 (t, *J* = 5.7 Hz, 1H), 6.68 (s, 1H), 6.37 (s, 1H), 5.84 (s, 2H), 4.59 (s, 1H), 3.26 (d, *J* = 6.1 Hz, 2H), 3.07 (d, *J* = 6.2 Hz, 2H), 2.46–2.18 (m, 4H), 1.59–1.41 (m, 6H), 1.36 (s, 9H). MS (ESI) *m/z* = 498.4 [*M* + H]⁺.

***N*-(4-(5,5-Difluoro-1,3,7,9-tetramethyl-5*H*-4λ⁴,5λ⁴-dipyrrolo[1,2-*c*:2',1'-*f*][1,3,2]diazaborinin-10-yl)-*N*-(2-(4-((6-hydroxybenzo[*d*][1,3]dioxol-5-yl)(piperidin-1-yl)methyl)benzamido)ethyl)benzamide (16).** To a solution of **S5** (11 mg, 0.022 mmol) in DCM (0.5 mL) was added TFA (0.05 mL), and the mixture was stirred at room temperature for 3 h. The mixture was concentrated and dissolved in DMF (0.5 mL). 4-(5,5-Difluoro-1,3,7,9-tetramethyl-

1
2
3 5*H*-4 λ^4 ,5 λ^4 -dipyrrolo[1,2-*c*:2',1'-*f*][1,3,2]diazaborinin-10-yl)benzoic acid (8 mg, 0.022 mmol,
4 synthesized by reported method), HATU (12.5 mg, 0.033 mmol), and DIEA (8.5 mg, 0.066 mmol)
5 were added subsequently. The mixture was stirred at room temperature overnight and partitioned
6 between EtOAc and water. The organic layer was washed with water twice, brine once, and dried
7 over anhydrous Na₂SO₄. The mixture was then filtered and concentrated. The residue was purified
8 with prep-HPLC (acetonitrile/water (10–95%)) over 25 min at an 8 mL/min flow rate at room
9 temperature) to give **16** as a red solid (3.0 mg, 18%). ¹H NMR (400 MHz, DMSO-*d*₆) δ 8.75 (s,
10 1H), 8.55 (s, 1H), 8.02 (d, *J* = 8.0 Hz, 2H), 7.77 (d, *J* = 8.0 Hz, 2H), 7.48 (dd, *J* = 12.5, 8.1 Hz,
11 4H), 6.68 (s, 1H), 6.37 (s, 1H), 6.20 (s, 2H), 5.83 (d, *J* = 1.2 Hz, 2H), 4.59 (s, 1H), 2.70–2.66 (m,
12 2H), 2.46 (s, 3H), 2.35–2.32 (m, 2H), 2.28 (dd, *J* = 11.9, 5.2 Hz, 4H), 1.55–1.38 (m, 6H), 1.33 (s,
13 3H). MS (ESI) *m/z* = 748.2 [M + H]⁺. Purity 96.1%.

14
15
16
17
18
19
20
21
22
23
24
25
26
27
28
29
30
31
32 **Cell Culture.** Human glioblastoma cells U-87 MG, U-118 MG, A-172, and MIA PaCa-2 were
33 obtained from the ATCC (Manassas, VA), and U-118 MG, A-172, and MIA PaCa-2 were
34 maintained in RPMI-1640 (Thermo Fisher Scientific, Waltham, MA) supplemented with 10%
35 fetal bovine serum (FBS) (Thermo Fisher Scientific). Dulbecco's phosphate-buffered saline
36 (DPBS) was purchased from Thermo Fisher Scientific. U-87 MG cells were maintained in DMEM
37 supplemented with 10% FBS. Cells were grown as monolayer cultures at 37 °C in a humidified
38 atmosphere of 5% CO₂ and tested for *Mycoplasma* contamination with the *Mycoplasma* detection
39 kit, Plasmotest (InvivoGen, San Diego, California). All cell lines were authenticated with STR
40 DNA profiling (University of Michigan, Michigan, USA) and matched to reference profiles from
41 the ATCC database. 3-(4,5-dimethylthiazol-2-yl)-2, 5-diphenyltetrazolium bromide (MTT) was
42 purchased from Amresco (Solon, OH). Small molecule screening libraries were purchased from
43
44
45
46
47
48
49
50
51
52
53
54
55
56
57
58
59
60

1
2
3 ChemDiv (San Diego, CA) or obtained from the National Cancer Institute through the
4
5
6 Developmental Therapeutics Program.

7
8 **PDI Protein Purification.** The expression vector of recombinant human wild-type PDI protein
9
10 with N-terminal His tag was a gift from Dr. Lloyd W. Ruddock (University of Oulu, Oulu,
11
12 Finland). Full-length recombinant PDI and the a'c domain (residues V360 – L499) were expressed
13
14 and purified as previously described⁹ with slight modifications. In brief, protein production was
15
16 carried out in *Escherichia coli* strain BL21 (DE3) grown in LB medium with 200 µg/ml ampicillin
17
18 (EMD Biosciences, La Jolla, CA) at 37 °C and incubated at an A_{600} of 0.5 for 4 h with 1 mM
19
20 isopropyl β-D-1-thiogalactopyranoside (GoldBio, St. Louis, MO). Cells were harvested by
21
22 centrifugation (2500g for 15 min) and were resuspended in 20 mM sodium phosphate, pH 7.3
23
24 buffer. Cells were lysed by sonication and the cell debris was removed by centrifugation (17000g
25
26 for 45 min). The supernatant was applied to a bed of Ni-nitrilotriacetic acid in a histidine-binding
27
28 column (Qiagen, Hilden, Germany), equilibrated with 10 ml of 20 mM sodium phosphate, pH 7.3
29
30 and incubated at 4 °C, overnight. After incubation, the column was washed in 20 mM sodium
31
32 phosphate, pH 7.3 and then in 20 mM sodium phosphate, 0.5 M sodium chloride and 20 mM
33
34 imidazole, pH 7.3. His-tagged proteins were eluted with a buffer containing 20 mM sodium
35
36 phosphate and 500 mM imidazole, pH 7.3, and eluent was dialyzed in 100 mM sodium phosphate
37
38 buffer (pH 7.0) with 2 mM EDTA. PDIA2 and PDIA3 were purified as described previously.³⁰
39
40
41
42
43
44

45
46 **Site-directed Mutagenesis.** H256A and C53S mutants of PDI were obtained using wild-type
47
48 PDI as the DNA template with the QuikChange II XL Site Directed Mutagenesis kit (Agilent
49
50 Technologies, Santa Cruz, CA). Procedure was performed according to the manufacturer's
51
52 protocol. All constructs were sequenced for verification and no additional mutations were
53
54
55
56
57
58
59
60

1
2
3 observed. Mutant PDI constructs were transformed into BL21 DE(3) cells and purified according
4 to the wild-type PDI purification protocol.
5
6

7
8 **PDI Reductase Assay.** PDI activity was assessed by measuring the PDI-catalyzed reduction of
9 insulin as described previously.¹⁷ In brief, recombinant PDI protein (0.4 μM or 50 nM for PDIA1,
10 1.6 μM PDIA2 or PDIA3) was incubated with indicated compounds at 37 °C for 1 h in sodium
11 phosphate buffer (100 mM sodium phosphate, 2 mM EDTA, 8 μM DTT, pH 7.0). A mixture of
12 sodium phosphate buffer, DTT (500 μM or 125 μM for 50 nM PDI reaction), and bovine insulin
13 (130 μM; Gemini BioProducts, West Sacramento, CA) was added to the incubated PDI protein.
14 The reduction reaction was catalyzed by PDI at room temperature, and the resulting aggregation
15 of reduced insulin B chains was measured at 620 nm. PDI activity was calculated with the formula,
16 PDI activity (%) = $[(OD_{T60[PDI+DTT+compound]} - OD_{T0[PDI+DTT+compound]}) - (OD_{T60[DTT]} - OD_{T0[DTT]})] /$
17 $[(OD_{T60[PDI+DTT]} - OD_{T0[PDI+DTT]}) - (OD_{T60[DTT]} - OD_{T0[DTT]})] \times 100$ (OD_{T0} and OD_{T60} were the
18 absorbance values at 0 and 60 min after the reduction reaction, respectively). For reactions
19 containing 50 nM PDI, PDI activity was measured at T180, or 180 min after insulin was added.
20
21
22
23
24
25
26
27
28
29
30
31
32
33
34
35
36

37 To determine the k_{inact}/K_I of covalent PDI inhibitors, the published procedure was adapted
38 with the following modifications.⁹ Compounds were incubated at 13.2 μM, 19.8 μM, 29.6 μM,
39 44.4 μM, 66.7 μM, 100 μM, and 150 μM for 5, 15, 30, 45, or 60 min before addition of the insulin
40 solution. The linear portions of the slopes of each kinetic curve obtained were used to calculate
41 the K_{obs} in GraphPad Prism. The k_{obs} at each concentration was plotted to obtain the slope of the
42 linear portion of the line as k_{inact}/K_I .
43
44
45
46
47
48
49
50
51

52 **Growth Inhibition Assay.** Cell growth inhibition was assessed by MTT assay as previously
53 described.⁶¹ Cells were seeded in duplicate in 96-well plates at 3000 – 5000 cells/well. After
54
55
56
57

1
2
3 overnight incubation at 37 °C and 5% CO₂, cells were treated with indicated compounds for 72 h.
4
5 For glutathione depletion experiments, cells were pretreated for 24 h with buthionine sulfoximine
6
7 (1 mM in A-172 or 4 μM in U-118 MG) before compound addition. MTT solution (20 μL 3
8
9 mg/mL) was added to the wells, and the cells were incubated for 4 h at 37 °C. Supernatant was
10
11 removed and DMSO (100 μl) was added to each well. The plates were shaken for 15 min at room
12
13 temperature and absorbance of the formazan crystals was measured at 570 nm. Cell growth
14
15 inhibition was assessed by the cell viability rate as $[1-(A_t-A_b)/(A_c-A_b)]\times 100$ (A_t , A_c and A_b were
16
17 the absorbance values from cells treated with compound, cells not treated with compound, and
18
19 blank, respectively).
20
21
22
23
24

25 **Colony Formation Assay.** Briefly, 600 U-118 MG or A-172 cells were seeded per well in
26
27 96-well plates and allowed to attach. After 24 h, serial dilutions of buthionine sulfoximine (Sigma)
28
29 were added. Cells were incubated overnight, and serial dilutions of experimental compounds were
30
31 added to the culture medium. Cells were cultured until colonies formed (10–14 days), stained with
32
33 crystal violet solution (0.25% crystal violet, 10% formaldehyde (37% v/v), 80% methanol) for 1
34
35 h, and thoroughly washed with water before imaging.
36
37
38

39 **Thermal Shift Assay.** Thermal shift of purified PDI (0.3 mg/ml in 100 mM NaPO₄, pH 7.0) in
40
41 the presence or absence of indicated compounds was determined as described.¹⁸ Briefly, PDI, 100
42
43 μM compound or DMSO as a vehicle control, 1X ROX dye, and 5 μl Protein Thermal Shift Buffer
44
45 were mixed to a 20 μl total volume in a 384-well microplate. Each reaction was repeated in
46
47 quadruplicate and reactions were mixed before measurements were taken. The plate was heated
48
49 from 25 to 90 °C at 0.05 °C/second with the ViiA 7 Real-Time PCR System (Thermo Fisher
50
51 Scientific, Waltham, MO). Melt curves were analyzed with the Protein Thermal Shift software
52
53 (Thermo Fisher Scientific) and Boltzmann melting temperatures were reported.
54
55
56
57
58
59
60

1
2
3 **Reversibility Assay.** PDI activity was assessed by measuring the PDI-catalyzed reduction of
4 insulin as described previously.¹⁷ In brief, 0.4 μM recombinant PDI was incubated with
5 compounds at indicated concentrations at 37 $^{\circ}\text{C}$ for 1 h in sodium phosphate buffer (100 mM
6 sodium phosphate, 2 mM EDTA, 8 μM DTT, pH 7.0). For samples containing diluted
7
8 protein-compound complexes, 40 μM PDI was incubated with 100 μM **PACMA31**, 50 μM
9
10 **BAP2**, 50 μM **AS15**, or 50 μM **CD343** for 3 h at room temperature, or was incubated with
11
12 400 μM **AS15**, 400 μM **CD343**, or 400 μM **6a** for 30 min at room temperature. The mixtures
13
14 were diluted 100-fold into buffer (100 mM sodium phosphate, 2 mM EDTA, 8 μM DTT, pH
15
16 7.0) and added to the 384-well, black, clear-bottom plate. A mixture of sodium phosphate
17
18 buffer, DTT (500 μM), and bovine insulin (130 μM ; Gemini BioProducts, West Sacramento, CA)
19
20 was added to the incubated PDI-compound samples. The reduction reaction was catalyzed by PDI
21
22 at room temperature, and the resulting aggregation of reduced insulin B chains was measured at
23
24 620 nm. Absorbance at 620 nm was measured in a 384-well black-walled, clear-bottom plate.
25
26
27
28
29
30
31
32
33
34
35
36
37
38
39
40

41 **1-Anilinonaphthalene-8-sulfonic acid (ANS) spectral scan.** The ANS spectral scan was
42 performed as previously described.³² Briefly, 5 μM PDI was incubated in the presence 100 μM
43 compounds or equivalent DMSO concentration in 50 μL of TBS at 37 $^{\circ}\text{C}$ for 1 h. Subsequently,
44 50 mM ANS was added and the mixture was incubated in the dark at 25 $^{\circ}\text{C}$ for 20 min.
45
46 Fluorescence spectrum (Ex: 370 nm, Em: 400–700 nm) was measured in a 384-well black-walled,
47
48 clear-bottom plate.
49
50
51
52
53
54
55
56
57
58
59
60

1
2
3 **Bromouridine RNA sequencing (Bru-seq).** Bru-seq was performed as previously described.⁵⁴

4 U-87MG cells were treated with DMSO or **5p** (20 μ M) for 4 h. Then 2 mM Bru was added in
5
6 the last 30 min of treatment. Cells were collected, and total RNA was isolated with TRIzol
7
8 reagent. Bru-labeled RNA was captured from total RNA by incubation with anti-BrdU
9
10 antibodies (BD Biosciences) conjugated to magnetic beads (Dynabeads, goat antimouse IgG;
11
12 Invitrogen). Bru-containing RNA population was isolated and sequenced. Sequencing reads
13
14 were mapped to the hg38 reference genome. Preranked gene lists were generated for each
15
16 treatment ranking genes by fold change in transcription compared to control. Sequencing results
17
18 were filtered using cutoff value of gene size > 300 bp and mean RPKM > 0.5.
19
20
21
22
23

24 The data sets were interrogated with Gene Set Enrichment Analysis (GSEA).⁵⁵ A log₂(fold
25
26 change) preranked gene list of 7,908 genes was analyzed for gene enrichment using GSEA gene
27
28 sets based on the Kolmogorov-Smirnov statistic. For each gene set, an enrichment score (ES) was
29
30 normalized to account for the difference in gene set size, and the false discovery rate (FDR) was
31
32 calculated based on the normalized enrichment score (NES) values.
33
34
35

36 The datasets were also interrogated with Connectivity Map (CMap,
37
38 <https://www.broadinstitute.org/connectivity-map-cmap>). Bru-seq gene sets were used with a cut
39
40 off of ≥ 2 -fold change in transcription. Some genes were omitted from analysis because there was
41
42 no connection in CMap.
43
44
45

46 **Western blot.** Cells were harvested with a lysis buffer (25 mM
47
48 tris(hydroxymethyl)aminomethane, 150 mM NaCl, 17 mM Triton X-100, 3.5 mM SDS, pH 7.4),
49
50 lysed via sonication, and spun in a centrifuge at 13,500g at 4 °C for 10 min. Supernatant was
51
52 collected and protein concentration determined with the BCA assay (Thermo Fisher Scientific,
53
54
55
56
57
58
59
60

1
2
3 Waltham, MO). Samples were prepared with 30 μg protein and loaded onto 10% acrylamide
4 (Bio-Rad, Hercules, CA) gels. Protein from gels was electrotransferred to methanol-activated
5 immobilon-FL PVDF membranes (EMD Millipore, La Jolla, CA). Membranes were blocked for
6 1 h with Odyssey blocking buffer (LI-COR Biosciences, Lincoln, NE). Membranes were probed
7 for proteins using primary antibodies (PDI, Cell Signaling, Danvers, MA, 1:1000) overnight at 4
8 $^{\circ}\text{C}$. Membranes were incubated with secondary antibodies (antirabbit, Cell Signaling, 1:7500, or
9 antimouse, Cell Signaling, 1:7500), and fluorescence was imaged by Odyssey imaging system
10 (LI-COR Biosciences).

11
12
13
14
15
16
17
18
19
20
21
22
23 **Proteomics.** U-118 MG cells were seeded in a 6-well plate at 0.5×10^6 cells/well in RPMI
24 supplemented with 10% FBS and allowed to attach overnight. Cells were treated with DMSO or
25 40 μM **15** overnight. Cells were washed with PBS and harvested with CelLytic M buffer (Sigma).
26 The cells were lysed by incubation for 1 h on ice and spun in a centrifuge at 13,500g at 4 $^{\circ}\text{C}$ for
27 10 min. Supernatant was collected and protein concentration determined with the BCA assay
28 (Thermo Fisher Scientific, Waltham, MO). Samples were prepared with 50 μg protein boiled with
29 Laemmli sample buffer and loaded onto 1 mm 10% acrylamide gels. The gel was immediately
30 imaged on the iBright with the GFP channel and stained with Coomassie. The band containing the
31 BODIPY-labeled compound was cut out, digested, and analyzed at the University of Michigan
32 Proteomics Resource Facility in the Department of Pathology.

33
34
35
36
37
38
39
40
41
42
43
44
45
46
47 **Confocal Imaging.** A-172 cells were treated with 10 μM **15** or 2 μM **16** overnight. Cells were
48 fixed in 4% paraformaldehyde for 15 min at room temperature and washed with 1X PBS before
49 blocking in 10% fetal bovine serum for 60 min. PDI antibody (Cell Signaling; 3501S) was applied
50 at 1:100 dilution in overnight at 4 $^{\circ}\text{C}$. ProLong Diamond with DAPI (Invitrogen) was used to
51 prepare the slides for analysis on the ZEISS Laser Scanning Microscope.

1
2
3 **Gel-based Binding Assays.** Gel-based binding assays were performed with recombinant protein
4 and cell lysate, as indicated. Briefly, cells were coated in 6-well or 12-well plates. After overnight
5 attachment, cells were either serum-starved, treated with BSO, or treated with test compounds at
6 indicated concentrations overnight at 37 °C, 5% CO₂. Cells were then washed with PBS and lysed
7 using CelLytic M buffer (Sigma) for 60 min on ice. A unit of 30–50 µg of whole-cell protein was
8 boiled with Laemmli sample buffer or non-reducing sample buffer (62.5 mM Tris-HCl, pH 6.8,
9 10% glycerol, 2% SDS, 0.05% bromophenol blue) and resolved on a 10% polyacrylamide gel.
10 Gels were immediately imaged on an iBright imaging system (Thermo Fisher Scientific). For cell
11 lysates, cells were harvested as above prior to compound treatment, then incubated with
12 compounds overnight at room temperature before subjecting to SDS PAGE. Similarly, *in vitro*
13 binding assays with recombinant PDIA1, PDIA2, PDIA3, and BSA were performed using 3.5 µM
14 protein in CelLytic M buffer incubated with compounds overnight at room temperature.
15
16
17
18
19
20
21
22
23
24
25
26
27
28
29
30

31 **Statistical analysis.** The IC₅₀ values were calculated using GraphPad Prism 7 software (GraphPad
32 Software, Inc.). The error bars indicate mean ± standard deviation. Bru-seq experiments were
33 performed once.
34
35
36
37
38
39

40 **Author Contributions.** #A. S. and D. X. contributed equally to this work. The manuscript
41 was written through contributions of all authors. All authors have given approval to the
42 final version of the manuscript.
43
44
45
46
47
48
49
50

51 **Acknowledgments.** The expression vectors of recombinant human PDI was generous gifts from
52 Dr. Lloyd W. Ruddock (University of Oulu, Oulu, Finland). The a'c domain vector was a kind gift
53 from Dr. C. C. Wang. We are grateful to Michelle Paulsen for performing the Bru-Seq
54
55
56
57
58
59
60

1
2
3 experiments and to Jennifer Schmidt for assistance with the Q–TOF mass spectrometry
4
5 experiments. We would also like to thank the University of Michigan Proteomics Resource Facility
6
7 at the Department of Pathology for performing the proteomics experiments and analyzing the
8
9 results and the University of Michigan DNA Sequencing Core. This work was supported by a grant
10
11 from the NIH (CA193690).
12
13

14 15 16 **Abbreviations Used**

17
18 CNS, central nervous system; DTT, dithiothreitol; PDI, protein disulfide isomerase; ROS, reactive
19
20 oxygen species; UPR, unfolded protein response. ATCC, American Type Culture Collection;
21
22 DMEM, Dulbecco’s Modified Eagle Medium; ER, endoplasmic reticulum; FBS, fetal bovine
23
24 serum; GBM, glioblastoma; GRP78, glucose–regulated protein, 78 kDa; LB, lysogeny broth; MTT,
25
26 3-(4,5-dimethylthiazol-2-yl)-2,5-diphenyltetrazolium bromide; NCI, National Cancer Institute;
27
28 PVDF, polyvinylidene difluoride; RPMI, Roswell Park Memorial Institute; STR, short tandem
29
30 repeats
31
32
33

34 35 **Corresponding Author**

36
37
38 *Phone: 734–647–2732. E–mail: neamati@umich.edu.
39
40
41

42
43 **Supporting Information.** Additional computational analysis, biochemical data, and
44
45 structures can be found in the Supporting Information. This material is available free of
46
47 charge via the Internet at <http://pubs.acs.org>.
48
49
50

51
52
53 **Supporting Information**
54
55
56
57
58
59
60

1
2
3 Supplemental File 1 - Proteomics
4
5

6 Supplemental File 2 - Bru-seq
7
8

9 Molecular Formula Strings: jmcmar_mfs_AS15_analogues
10
11
12
13
14
15
16
17
18
19
20
21
22
23
24
25
26
27
28
29
30
31
32
33
34
35
36
37
38
39
40
41
42
43
44
45
46
47
48
49
50
51
52
53
54
55
56
57
58
59
60

References

1. Ostrom, Q. T.; Cioffi, G.; Gittleman, H.; Patil, N.; Waite, K.; Kruchko, C.; Barnholtz-Sloan, J. S. CBTRUS statistical report: Primary brain and other central nervous system tumors diagnosed in the United States in 2012-2016. *Neuro Oncol* **2019**, *21*, v1-v100.
2. Shergalis, A.; Bankhead, A., 3rd; Luesakul, U.; Muangsin, N.; Neamati, N. Current challenges and opportunities in treating glioblastoma. *Pharmacol Rev* **2018**, *70*, 412-445.
3. Wang, C.; Li, W.; Ren, J.; Fang, J.; Ke, H.; Gong, W.; Feng, W.; Wang, C. C. Structural insights into the redox-regulated dynamic conformations of human protein disulfide isomerase. *Antioxid. Redox Signal.* **2013**, *19*, 36-45.
4. Zou, H.; Wen, C.; Peng, Z.; Shao, Y.; Hu, L.; Li, S.; Li, C.; Zhou, H. H. P4HB and PDIA3 are associated with tumor progression and therapeutic outcome of diffuse gliomas. *Oncol. Rep.* **2018**, *39*, 501-510.
5. Lee, D.; Sun, S.; Ho, A. S.; Kiang, K. M.; Zhang, X. Q.; Xu, F. F.; Leung, G. K. Hyperoxia resensitizes chemoresistant glioblastoma cells to temozolomide through unfolded protein response. *Anticancer Res.* **2014**, *34*, 2957-2966.
6. Xu, S.; Sankar, S.; Neamati, N. Protein disulfide isomerase: A promising target for cancer therapy. *Drug Discov. Today* **2014**, *19*, 222-240.
7. Lappi, A. K.; Lensink, M. F.; Alanen, H. I.; Salo, K. E.; Lobell, M.; Juffer, A. H.; Ruddock, L. W. A conserved arginine plays a role in the catalytic cycle of the protein disulphide isomerases. *J. Mol. Biol.* **2004**, *335*, 283-295.
8. Xu, S.; Butkevich, A. N.; Yamada, R.; Zhou, Y.; Debnath, B.; Duncan, R.; Zandi, E.; Petasis, N. A.; Neamati, N. Discovery of an orally active small-molecule irreversible inhibitor of

1
2
3 protein disulfide isomerase for ovarian cancer treatment. *Proc. Natl. Acad. Sci. U S A* **2012**, 109,
4
5 16348-16353.

6
7
8 9. Cole, K. S.; Grandjean, J. M. D.; Chen, K.; Witt, C. H.; O'Day, J.; Shoulders, M. D.;
9
10 Wiseman, R. L.; Weerapana, E. Characterization of an A-site selective protein disulfide
11
12 isomerase A1 inhibitor. *Biochemistry* **2018**, 57, 2035-2043.

13
14
15 10. Chen, I. H.; Chang, F. R.; Wu, Y. C.; Kung, P. H.; Wu, C. C. 3,4-Methylenedioxy-beta-
16
17 nitrostyrene inhibits adhesion and migration of human triple-negative breast cancer cells by
18
19 suppressing beta1 integrin function and surface protein disulfide isomerase. *Biochimie* **2015**,
20
21 110, 81-92.

22
23
24 11. Hoffstrom, B. G.; Kaplan, A.; Letso, R.; Schmid, R. S.; Turmel, G. J.; Lo, D. C.;
25
26 Stockwell, B. R. Inhibitors of protein disulfide isomerase suppress apoptosis induced by
27
28 misfolded proteins. *Nat. Chem. Biol.* **2010**, 6, 900-906.

29
30
31 12. Xu, S.; Butkevich, A. N.; Yamada, R.; Zhou, Y.; Debnath, B.; Duncan, R.; Zandi, E.;
32
33 Petasis, N. A.; Neamati, N. Discovery of an orally active small-molecule irreversible inhibitor of
34
35 protein disulfide isomerase for ovarian cancer treatment. *Proc. Natl. Acad. Sci. U. S. A.* **2012**,
36
37 109, 16348-16353.

38
39
40 13. Won, J. K.; Yu, S. J.; Hwang, C. Y.; Cho, S. H.; Park, S. M.; Kim, K.; Choi, W. M.; Cho,
41
42 H.; Cho, E. J.; Lee, J. H.; Lee, K. B.; Kim, Y. J.; Suh, K. S.; Jang, J. J.; Kim, C. Y.; Yoon, J. H.;
43
44 Cho, K. H. Protein disulfide isomerase inhibition synergistically enhances the efficacy of
45
46 sorafenib for hepatocellular carcinoma. *Hepatology* **2017**, 66, 855-868.

47
48
49 14. Foster, C. K.; Thorpe, C. Challenges in the evaluation of thiol-reactive inhibitors of
50
51 human protein disulfide Isomerase. *Free Radic. Biol. Med.* **2017**, 108, 741-749.

- 1
2
3 15. Long, M. J. C.; Aye, Y. Privileged electrophile sensors: A resource for covalent drug
4 development. *Cell Chem. Biol.* **2017**, *24*, 787-800.
5
6
7
8 16. Ogunrinu, T. A.; Sontheimer, H. Hypoxia increases the dependence of glioma cells on
9 glutathione. *J. Biol. Chem.* **2010**, *285*, 37716-37724.
10
11
12 17. Lv, H.; Zhen, C.; Liu, J.; Yang, P.; Hu, L.; Shang, P. Unraveling the potential role of
13 glutathione in multiple forms of cell death in cancer therapy. *Oxid. Med. Cell Longev.* **2019**,
14 2019, 3150145.
15
16
17
18 18. Montero, D.; Tachibana, C.; Rahr Winther, J.; Appenzeller-Herzog, C. Intracellular
19 glutathione pools are heterogeneously concentrated. *Redox Biol.* **2013**, *1*, 508-513.
20
21
22 19. Boskovic, Z. V.; Kemp, M. M.; Freedy, A. M.; Viswanathan, V. S.; Pop, M. S.; Fuller, J.
23 H.; Martinez, N. M.; Figueroa Lazu, S. O.; Hong, J. A.; Lewis, T. A.; Calarese, D.; Love, J. D.;
24 Vetere, A.; Almo, S. C.; Schreiber, S. L.; Koehler, A. N. Inhibition of zinc-dependent histone
25 deacetylases with a chemically triggered electrophile. *ACS Chem. Biol.* **2016**, *11*, 1844-1851.
26
27
28 20. McLean, L. R.; Zhang, Y.; Li, H.; Li, Z.; Lukasczyk, U.; Choi, Y. M.; Han, Z.; Prisco, J.;
29 Fordham, J.; Tsay, J. T.; Reiling, S.; Vaz, R. J.; Li, Y. Discovery of covalent inhibitors for MIF
30 tautomerase via cocrystal structures with phantom hits from virtual screening. *Bioorg. Med.*
31 *Chem. Lett.* **2009**, *19*, 6717-6720.
32
33
34 21. Zapatero, M. C.; Perez, P.; Vazquez, M. J.; Colmenarejo, G.; de Los Frailes, M.; Ramon,
35 F. Discovery of novel inhibitors of the tautomerase activity of macrophage migration inhibitory
36 factor (MIF). *J. Biomol. Screen.* **2016**, *21*, 446-458.
37
38
39 22. Ouertatani-Sakouhi, H.; El-Turk, F.; Fauvet, B.; Cho, M. K.; Pinar Karpinar, D.; Le Roy,
40 D.; Dewor, M.; Roger, T.; Bernhagen, J.; Calandra, T.; Zweckstetter, M.; Lashuel, H. A.
41
42
43
44
45
46
47
48
49
50
51
52
53
54
55
56
57
58
59
60

- 1
2
3 Identification and characterization of novel classes of macrophage migration inhibitory factor
4 (MIF) inhibitors with distinct mechanisms of action. *J. Biol. Chem.* **2010**, 285, 26581-26598.
5
6
7 23. Cisneros, J. A.; Robertson, M. J.; Valhondo, M.; Jorgensen, W. L. Irregularities in
8 enzyme assays: The case of macrophage migration inhibitory factor. *Bioorg. Med. Chem. Lett.*
9
10 **2016**, 26, 2764-2767.
11
12
13 24. Jiang, X.; Hu, C.; Ferchen, K.; Nie, J.; Cui, X.; Chen, C. H.; Cheng, L.; Zuo, Z.; Seibel,
14 W.; He, C.; Tang, Y.; Skibbe, J. R.; Wunderlich, M.; Reinhold, W. C.; Dong, L.; Shen, C.;
15
16
17
18
19
20
21
22
23
24
25
26
27
28
29
30
31
32
33
34
35
36
37
38
39
40
41
42
43
44
45
46
47
48
49
50
51
52
53
54
55
56
57
58
59
60
25. Lavecchia, A.; Di Giovanni, C.; Cerchia, C.; Russo, A.; Russo, G.; Novellino, E.
Discovery of a novel small molecule inhibitor targeting the frataxin/ubiquitin interaction via
structure-based virtual screening and bioassays. *J. Med. Chem.* **2013**, 56, 2861-2873.
26. Thinnes, C. C.; Tumber, A.; Yapp, C.; Scozzafava, G.; Yeh, T.; Chan, M. C.; Tran, T. A.;
Hsu, K.; Tarhonskaya, H.; Walport, L. J.; Wilkins, S. E.; Martinez, E. D.; Muller, S.; Pugh, C.
W.; Ratcliffe, P. J.; Brennan, P. E.; Kawamura, A.; Schofield, C. J. Betti reaction enables
efficient synthesis of 8-hydroxyquinoline inhibitors of 2-oxoglutarate oxygenases. *Chem.*
Commun. (Camb.) **2015**, 51, 15458-15461.
27. Olyaei, A.; Sadeghpour, M. Recent advances in the synthesis and synthetic applications
of Betti base (aminoalkyl naphthol) and bis-Betti base derivatives. *RSC Adv.* **2019**, 9, 18467-
18497.

- 1
2
3 28. Wu, B.; Gao, X.; Yan, Z.; Chen, M. W.; Zhou, Y. G. C-H oxidation/Michael
4 addition/cyclization cascade for enantioselective synthesis of functionalized 2-amino-4H-
5 chromenes. *Org. Lett.* **2015**, *17*, 6134-6137.
6
7
8
9
10 29. Sartori, G.; Casnati, G.; Bigi, F.; Predieri, G. Ortho-coordinated acylation of phenol
11 systems. *J. Org. Chem.* **1990**, *55*, 4371-4377.
12
13
14 30. Xu, S.; Liu, Y.; Yang, K.; Wang, H.; Shergalis, A.; Kyani, A.; Bankhead, A., 3rd;
15 Tamura, S.; Yang, S.; Wang, X.; Wang, C. C.; Rehemtulla, A.; Ljungman, M.; Neamati, N.
16 Inhibition of protein disulfide isomerase in glioblastoma causes marked downregulation of DNA
17 repair and DNA damage response genes. *Theranostics* **2019**, *9*, 2282-2298.
18
19
20 31. Madonna, S.; Beclin, C.; Laras, Y.; Moret, V.; Marcowycz, A.; Lamoral-Theys, D.;
21 Dubois, J.; Barthelemy-Requin, M.; Lenglet, G.; Depauw, S.; Cresteil, T.; Aubert, G.; Monnier,
22 V.; Kiss, R.; David-Cordonnier, M. H.; Kraus, J. L. Structure-activity relationships and
23 mechanism of action of antitumor bis 8-hydroxyquinoline substituted benzylamines. *Eur. J. Med.*
24 *Chem.* **2010**, *45*, 623-638.
25
26
27 32. Bekendam, R. H.; Bendapudi, P. K.; Lin, L.; Nag, P. P.; Pu, J.; Kennedy, D. R.;
28 Feldenzer, A.; Chiu, J.; Cook, K. M.; Furie, B.; Huang, M.; Hogg, P. J.; Flaumenhaft, R. A
29 substrate-driven allosteric switch that enhances PDI catalytic activity. *Nat. Commun.* **2016**, *7*,
30 12579.
31
32
33 33. Go, Y. M.; Jones, D. P. Redox compartmentalization in eukaryotic cells. *Biochim.*
34 *Biophys. Acta* **2008**, *1780*, 1273-1290.
35
36
37 34. Walker, K. W.; Gilbert, H. F. Oxidation of kinetically trapped thiols by protein disulfide
38 isomerase. *Biochemistry* **1995**, *34*, 13642-13650.
39
40
41
42
43
44
45
46
47
48
49
50
51
52
53
54
55
56
57
58
59
60

- 1
2
3 35. Paulsen, M. T.; Veloso, A.; Prasad, J.; Bedi, K.; Ljungman, E. A.; Magnuson, B.; Wilson,
4 T. E.; Ljungman, M. Use of Bru-Seq and BruChase-Seq for genome-wide assessment of the
5 synthesis and stability of RNA. *Methods* **2014**, *67*, 45-54.
6
7
8
9
10 36. Wang, W. A.; Groenendyk, J.; Michalak, M. Calreticulin signaling in health and disease.
11 *Int. J. Biochem. Cell Biol.* **2012**, *44*, 842-846.
12
13
14 37. Jessop, C. E.; Tavender, T. J.; Watkins, R. H.; Chambers, J. E.; Bulleid, N. J. Substrate
15 specificity of the oxidoreductase ERp57 is determined primarily by its interaction with calnexin
16 and calreticulin. *J. Biol. Chem.* **2009**, *284*, 2194-2202.
17
18
19
20 38. Wang, M.; Wey, S.; Zhang, Y.; Ye, R.; Lee, A. S. Role of the unfolded protein response
21 regulator GRP78/BiP in development, cancer, and neurological disorders. *Antioxid. Redox*
22 *Signal.* **2009**, *11*, 2307-2316.
23
24
25
26 39. Oh, E. T.; Park, H. J. Implications of NQO1 in cancer therapy. *BMB Rep.* **2015**, *48*, 609-
27 617.
28
29
30
31
32 40. Koppula, P.; Zhang, Y.; Zhuang, L.; Gan, B. Amino acid transporter SLC7A11/xCT at
33 the crossroads of regulating redox homeostasis and nutrient dependency of cancer. *Cancer*
34 *Commun. (Lond.)* **2018**, *38*, 12.
35
36
37
38 41. Kyani, A.; Tamura, S.; Yang, S.; Shergalis, A.; Samanta, S.; Kuang, Y.; Ljungman, M.;
39 Neamati, N. Discovery and mechanistic elucidation of a class of protein disulfide isomerase
40 inhibitors for the treatment of glioblastoma. *ChemMedChem* **2018**, *13*, 164-177.
41
42
43
44 42. Lamb, J.; Crawford, E. D.; Peck, D.; Modell, J. W.; Blat, I. C.; Wrobel, M. J.; Lerner, J.;
45 Brunet, J. P.; Subramanian, A.; Ross, K. N.; Reich, M.; Hieronymus, H.; Wei, G.; Armstrong, S.
46 A.; Haggarty, S. J.; Clemons, P. A.; Wei, R.; Carr, S. A.; Lander, E. S.; Golub, T. R. The
47
48
49
50
51
52
53
54
55
56
57
58
59
60

1
2
3 Connectivity Map: Using gene-expression signatures to connect small molecules, genes, and
4
5 disease. *Science* **2006**, 313, 1929-1935.
6

7
8 43. Nakamura, Y.; Feng, Q.; Kumagai, T.; Torikai, K.; Ohigashi, H.; Osawa, T.; Noguchi,
9
10 N.; Niki, E.; Uchida, K. Ebselen, a glutathione peroxidase mimetic seleno-organic compound, as
11
12 a multifunctional antioxidant. Implication for inflammation-associated carcinogenesis. *J. Biol.*
13
14 *Chem.* **2002**, 277, 2687-2694.
15

16
17 44. Bender, K. O.; Garland, M.; Ferreyra, J. A.; Hryckowian, A. J.; Child, M. A.; Puri, A.
18
19 W.; Solow-Cordero, D. E.; Higginbottom, S. K.; Segal, E.; Banaei, N.; Shen, A.; Sonnenburg, J.
20
21 L.; Bogoyo, M. A small-molecule antivirulence agent for treating *Clostridium difficile* infection.
22
23 *Sci. Transl. Med.* **2015**, 7, 306ra148.
24

25
26 45. Beilhartz, G. L.; Tam, J.; Zhang, Z.; Melnyk, R. A. Comment on "A small-molecule
27
28 antivirulence agent for treating *Clostridium difficile* infection". *Sci. Transl. Med.*
29
30
31 **2016**, 8, 370tc2.
32

33
34 46. Trychta, K. A.; Back, S.; Henderson, M. J.; Harvey, B. K. KDEL receptors are
35
36 differentially regulated to maintain the ER proteome under calcium deficiency. *Cell Rep.* **2018**,
37
38 25, 1829-1840.e6.
39

40
41 47. Schurmann, M.; Janning, P.; Ziegler, S.; Waldmann, H. Small-molecule target
42
43 engagement in cells. *Cell Chem. Biol.* **2016**, 23, 435-441.
44

45
46 48. Richard, D. J.; Lena, R.; Bannister, T.; Blake, N.; Pierceall, W. E.; Carlson, N. E.; Keller,
47
48 C. E.; Koenig, M.; He, Y.; Minond, D.; Mishra, J.; Cameron, M.; Spicer, T.; Hodder, P.;
49
50 Cardone, M. H. Hydroxyquinoline-derived compounds and analoging of selective Mcl-1
51
52 inhibitors using a functional biomarker. *Bioorg. Med. Chem.* **2013**, 21, 6642-6649.
53
54
55
56
57
58
59
60

- 1
2
3 49. Fu, R.; Ding, Y.; Luo, J.; Yu, L.; Li, C. L.; Li, D. S.; Guo, S. W. TET1 exerts its tumour
4
5 suppressor function by regulating autophagy in glioma cells. *Biosci. Rep.* **2017**, *37*, pii:
6
7 BSR20160523.
8
9
10 50. Bansal, A.; Simon, M. C. Glutathione metabolism in cancer progression and treatment
11
12 resistance. *J. Cell Biol.* **2018**, *217*, 2291-2298.
13
14 51. Zhu, Z.; Du, S.; Du, Y.; Ren, J.; Ying, G.; Yan, Z. Glutathione reductase mediates drug
15
16 resistance in glioblastoma cells by regulating redox homeostasis. *J. Neurochem.* **2018**, *144*, 93-
17
18 104.
19
20 52. Huang, Z. Z.; Chen, C.; Zeng, Z.; Yang, H.; Oh, J.; Chen, L.; Lu, S. C. Mechanism and
21
22 significance of increased glutathione level in human hepatocellular carcinoma and liver
23
24 regeneration. *FASEB J.* **2001**, *15*, 19-21.
25
26
27 53. Lu, S. C. Regulation of glutathione synthesis. *Mol. Aspects Med.* **2009**, *30*, 42-59.
28
29 54. Paulsen, M. T.; Veloso, A.; Prasad, J.; Bedi, K.; Ljungman, E. A.; Tsan, Y. C.; Chang, C.
30
31 W.; Tarrier, B.; Washburn, J. G.; Lyons, R.; Robinson, D. R.; Kumar-Sinha, C.; Wilson, T. E.;
32
33 Ljungman, M. Coordinated regulation of synthesis and stability of RNA during the acute TNF-
34
35 induced proinflammatory response. *Proc. Natl. Acad. Sci. U. S. A.* **2013**, *110*, 2240-2245.
36
37
38 55. Subramanian, A.; Tamayo, P.; Mootha, V. K.; Mukherjee, S.; Ebert, B. L.; Gillette, M.
39
40 A.; Paulovich, A.; Pomeroy, S. L.; Golub, T. R.; Lander, E. S.; Mesirov, J. P. Gene set
41
42 enrichment analysis: A knowledge-based approach for interpreting genome-wide expression
43
44 profiles. *Proc. Natl. Acad. Sci. U. S. A.* **2005**, *102*, 15545-15550.
45
46
47
48
49
50
51
52
53
54
55
56
57
58
59
60

Table of Contents graphic

